DESIGN OF FUNCTIONALIZABLE POLYMER COATED MAGNETIC NANOPARTICLES FOR DRUG DELIVERY APPLICATIONS

by

Yavuz Öz

B.S., Chemistry, Gazi University, 2010

Submitted to the Institute for Graduate Studies in
Science and Engineering in partial fulfillment of
the requirements for the degree of
Master of Science

Graduate Program in Chemistry

Bogazici University

2014

DESIGN OF FUNCTIONALIZABLE POLYMER COATED MAGNETIC NANOPARTICLES FOR DRUG DELIVERY APPLICATIONS

APPROVED BY:

Assoc. Prof. Amitav Sanyal ……..
(Thesis Supervisor)

Prof. Dr. Naci İnci ……...

Assoc. Prof. Rana Sanyal ……

DATE OF APPROVAL: 13.08.2014

Dedicated to my grandfather and my best friend İbrahim Hakkı Yıldırım

ACKNOWLEDGEMENTS

I would like to thank my thesis supervisor Assoc. Prof. Amitav Sanyal for his endless encouragement and support. Throughout the thesis, his positive attitude has been the most encouraging force for me to pursue my thesis with an ambition. I am so grateful for his contribution to my chemistry and experimental knowledge.

I would like to express my thanks to Assoc. Prof. Rana Sanyal for her recommendations regarding my life and research.

I wish to extend my thanks to Prof. Dr. Naci İnci for his careful and constructive review of the final manuscript and attending my defense jury.

I am so glad to work with enthusiastic and hardworking friends. I wish to express my great thanks to Tuğçe Nihal for her patience and helpfulness. Also, I want to thank Mehmet for his guidance on my thesis. I would like to thank Nergiz, Burcu, Janset, Harun, Filiz and Özgül for their friendship and the best memories. I would like to extend my thanks to Özlem, Hasancan, Laura, Duygu, Hazal, Merve, Sadık, Sesil, Yasemin, and ex-labmates Pelin, Merve, Aslı, Rabia, Merve, Nazlı and Sedef. I would like to thank my roommate Emrullah for his support and friendship from preparatory school to my master defense.

Finally, my deepest thanks go to my family for their love and support.

This research has been supported by The Scientific and Technological Research Council of Turkey (TÜBİTAK) (BİDEB – 2210-C), and Bogazici University Research Funds (BAP 13B05D4).

ABSTRACT

DESIGN OF FUNCTIONALIZABLE POLYMER COATED MAGNETIC NANOPARTICLES FOR DRUG DELIVERY APPLICATIONS

Synthesis of monodisperse, water-dispersible and biocompatible iron oxide nanoparticles with functional groups has gained importance because of the potential applications in biomedicine such as drug delivery, MRI agent, etc. In this thesis, azide and thiol end group reactive polymers containing iron oxide nanoparticles were examined. Catechol group containing chain transfer agent was immobilized onto oleic acid coated iron oxide nanoparticle surface by means of a place exchange modification. Poly(ethylene glycol) methyl ether acrylate (PEGMEA) monomer based hydrophilic polymers were synthesized using reversible addition-fragmentation chain transfer polymerization (RAFT) with graft-from approach. Polymer coated nanoparticles were characterized by fourier transform infrared (FT-IR), thermal gravimetric analysis (TGA) and dynamic light scattering (DLS). Nanoparticles were functionalized with azido and protected maleimide groups by post-polymerization modification technique. Thiocarbonylthio end groups that originates from RAFT agent was converted into furan protected maleimide and azido groups using radical cross-coupling reaction. Removal of the furan groups after modification of end groups gives thiol reactive nanoparticles. Similarly, azido group functionalization produces alkyne reactive polymer coated nanoparticles. Thiol and acetylene containing hydrophobic dyes were conjugated with maleimide and azido end groups containing nanoparticles, respectively. Fluorescent nanoparticles easily dispersed in water after dye conjugation.

ÖZET

İLAÇ TAŞIMA UYGULAMARI İÇİN FONKSİYONELLEŞTİRİLEBİLİR POLİMER KAPLI MANYETİK NANOPARÇACIKLARIN TASARIMI

Tekil dağılımlı, suda dağılabilen ve biyo uyumlu, fonksiyonel grup içeren demir oksit nanoparçacıklarının sentezi, ilaç taşıma, MRI ajanı gibi biyotıptaki potansiyel uygulamalarından dolayı önem kazandı. Bu tezde, uç gruplarında azit ve tiyol fonksiyonel gruplar olan reaktif polimerler içeren demir oksit nanoparçacıkları incelenmiştir. Katekol grubu içeren zincir transfer ajanı, oleik asit kaplanmış demir oksit nanoparçacıklarının yüzeyine yer değiştirme modifikasyonu ile sabitlenmiştir. Polietilen glikol metil eter akrilat monomer temelli hidrofilik polimerler, tersinir katılma-ayrışma zincir transfer polimerleşmesi kullanılarak, yüzeyden büyütme metoduyla sentezlendiler. Polimer kaplı nanoparçacıklar fourier transform infrared (FT-IR) spektroskopisi, termal gravimetrik analiz (TGA) ve dinamik ışık saçılması (DLS) ile karakterize edildi. Nanoparçacıklar azit ve korunmuş maleimit grupları ile polimerizasyon sonrası modifikasyon tekniği kullanılarak fonksiyonelleştirildi. RAFT ajanından kaynaklanan tiyokarbonil-tiyo uç grupları radikalik çapraz eşleşme reaksiyonu kullanılarak furan korunmuş maleimit ve azit gruplarına dönüştürüldü. Uç grupların modifikasyonundan sonra furan grubunun uzaklaştırılması tiyol reaktif nanoparçacıklar verir. Aynı şekilde, azit grup modifikasyonu alkin reaktif polimer kaplı nanoparçacıklar meydana getirir. Tiyol ve asetilen taşıyan hidrofobik boyalar sırasıyla maleimit ve azit uç gruplar içeren nanoparçacıklarla konjüge edildi. Boya konjügasyonundan sonra, floresan nanoparçacıklar kolaylıkla suda dağıldılar.

TABLE OF CONTENTS

ACKNOWLEDGEMENTS iv

ABSTRACT v

ÖZET vi

LIST OF FIGURES x

LIST OF TABLES xii

1. INTRODUCTION 1

1.1. Iron Oxide Nanoparticles 1

1.1.1. Synthetic Pathway of Iron Oxide Nanoparticles 2

1.1.1.1. Thermal Decomposition Procedure 3

1.2. Surface Modification of Iron Oxide Nanoparticles 4

1.2.1. Inorganic Materials 5

1.2.2. Organic Materials (Polymers) 6

1.2.2.1. Grafting-to Approach. 7

1.2.2.2. Grafting-from Approach. 9

1.3. Reversible Addition-Fragmentation Chain Transfer (RAFT) Polymerization 11

1.4. End Group Modification of RAFT Polymers 13

1.5. Click Type Chemistry 15

1.6. Maleimide-Thiol Michael Addition Reaction 16

2. AIM OF THE STUDY 18

3. EXPERIMENTAL 20

3.1. Materials 20

3.2. Measurements 20

3.3. Synthesis of Iron Oxide Nanoparticles 21

3.3.1. Synthesis of Iron Oleate Complex 21

3.3.2. Iron Oxide Nanoparticles by Thermal Decomposition Method 21
3.4. Preparation of Catechol Modified Chain Transfer Agent 22
3.4.1. Synthesis of 2-(Dodecylthiocarbonothioylthio)-2-methylpropanoic acid (DDMAT) 22
3.4.2. Synthesis of DDMAT Succinimide (DDMAT-NHS) Ester 22
3.4.3. Synthesis of Dopamine Terminated Chain Transfer Agent (Dopa-CTA) ... 23
3.5. Synthesis of 4,4'-azobis(azidohexanoyl 4-cyanopentanoate) 23
3.6. Synthesis of 4-(3-Hydroxypropyl)-10-oxa-4-azatricyclo[5,2,1,0]dec-8-ene-3,5 Dione 24
3.7. Ligand Exchange Procedure 24
3.8. Surface-Initiated RAFT Polymerization of PEGMA 25
3.9. End Group Modifications of Polymer Coated Magnetic Nanoparticles 25
3.9.1. End Group Modification with Furan Protected Maleimide Functional Groups 25
3.9.2. End Group Modification with Azide Functional Groups 25
3.10. Activation of Maleimide Functional Groups by Retro Diels-Alder Reaction 26
3.11. Dye Conjugations with Iron Oxide Nanoparticles 26
3.11.1. Dye Conjugation of Maleimide Containing Polymer Coated Magnetic Nanoparticles by Thiol-Ene Reaction 26
3.11.2. Dye Conjugation of Azido Containing Polymer Coated Magnetic Nanoparticles by Huisgen Cycloaddition 26
4. RESULTS AND DISCUSSIONS 27
4.1. Synthesis of Iron Oxide Nanoparticles 27
4.2. Modification of Chain Transfer Agent 28
4.3. Diazido-V-501 Compound 31
4.4. Synthesis of Protected Maleimide V501 Derivative 33

4.5. Chain Transfer Agent (CTA) Immobilization onto Magnetic Nanoparticles via Place Exchange Reaction 34
4.6. RAFT Polymerization of PEGMA with Grafting-From Manner 35
4.7. End Group Modifications of Polymer Coated NPs by Typical Radical Cross-Coupling Reaction 36
4.7.1. Modification with Protected Maleimide Azo-Initiator 36
4.7.2 Activation of Maleimide Groups by Retro Diels-Alder Reaction 38
4.7.3. Modification with Azido Bearing Azo-Initiator 40
4.8. Functionalization of Polymer Coated Nanoparticles 42
4.8.1. Nucleophilic Thiol-Ene Reaction 42
4.8.2. Huisgen Cyloaddition Reaction 43
4.10. Thermal Gravimetric Analysis of Iron Oxide NPs 44
4.11. Dynamic Light Scattering Measurements of Iron Oxide NPs 45
4.12. Transmission Electron Microscopy (TEM) 48
5. CONCLUSION 50
REFERENCES 51

LIST OF FIGURES

Figure 1.1. TEM images of (a) 12.5 nm (b) 17.6 nm and (c) 22.5 nm iron oxide nano-particles using octadecene, eicosane and docosane as solvents, respectively [25]..... 4
Figure 1.2. Most commonly used anchoring groups for iron oxide NPs..... 5
Figure 1.3. Dextran conjugation to amine functionalized silica coated NPs [37]..... 6
Figure 1.4. Polymer conjugation to iron oxide NP by grafting-to method..... 8
Figure 1.5. Preparation of the carboxyl- and catechol-PEG-derivatized oligomers and immobilization onto iron oxide NP surface [52]..... 9
Figure 1.6. Polymer conjugation to iron oxide NP by grafting-from method..... 10
Figure 1.7. Synthesis of Fe_3O_4@PHEMA-g-PCL magnetic NPs by ATRP and ROP [29]..... 10
Figure 1.8. General mechanism of RAFT polymerization..... 12
Figure 1.9. End group modification of RAFT polymer..... 13
Figure 1.10. Synthesis of biotin-maleimide heterotelechelic pNIPAAm and conjugation of SAv and BSA [73]..... 14
Figure 1.11. Commonly utilized ‘Click’ type reactions..... 15
Figure 1.12. Sequential one-pot photoinduced CuAAC and thiol-ene click reactions yielding bio-active block co-polymer [81]..... 16
Figure 1.13. Reaction scheme of preparation of maleimide-Au NPs and Michael addition of SiFA-SH and cysteine derivative cys-TATE peptide [84]..... 17
Figure 2.1. General scheme of the project..... 18
Figure 4.1. Synthetic route of iron oxide NPs..... 27
Figure 4.2. Oleic acid stabilized nanoparticles (a) FT-IR spectra (b) TEM image..... 28
Figure 4.3. Synthesis of dopamine terminated chain transfer agent..... 29
Figure 4.4. ^{1}H NMR spectrum of Dopa-CTA..... 30
Figure 4.5. ^{13}C NMR spectrum of Dopa-CTA..... 30
Figure 4.6. Two step synthesis of diazido-V-501 (1)..... 31
Figure 4.7. ^{1}H NMR spectrum of diazido-V-501..... 32
Figure 4.8. ^{13}C NMR spectrum of diazido-V-501..... 32

Figure 4.9. Synthesis of protected maleimide containing diazo compound (3). 33
Figure 4.10. (a) Dopa-CTA immobilization onto iron oxide NPs and (b) FT-IR spectra of Dopa-CTA coated iron oxide NPs. 34
Figure 4.11. (a) FT-IR spectra of polymer coated magnetic NPs (b) synthesis of p(PEGMA) coated iron oxide NPs. 35
Figure 4.12. End group modification of magnetic NPs by protected maleimide group and AIBN. 36
Figure 4.13. FT-IR spectra of furan protected maleimide terminated iron oxide NPs. 38
Figure 4.14. End group activation of magnetic NPs by retro Diels-Alder reaction. 39
Figure 4.15. FT-IR spectra of maleimide terminated iron oxide NPs. 40
Figure 4.16. End group modification of magnetic NPs by azido groups and AIBN. 41
Figure 4.17. FT-IR spectra of azido group terminated magnetic NPs 42
Figure 4.18. Dye conjugation onto maleimide groups terminated iron oxide NPs by thiol-ene chemistry (a) dye attached NPs (b) control (c) free dye. 43
Figure 4.19. Dye conjugation onto azido groups terminated iron oxide NPs by Huisgen click chemistry (a) dye attached NPs (b) control (c) free dye. 44
Figure 4.20. TGA curves of Fe_3O_4@OA, Fe_3O_4@CTA and Fe_3O_4@PEGMA 45
Figure 4.21. DLS analysis of iron oxide NPs (a) Fe_3O_4@OA (b) Fe_3O_4@CTA and (c) Fe_3O_4@PEGMA 46
Figure 4.22. DLS analysis of NPs (a) Fe_3O_4@PEGMA-pMAL3 (b) Fe_3O_4@PEGMA-MAL3 (c) Fe_3O_4@PEGMA@N_3-3 48
Figure 4.23. TEM images of magnetic NPs (a) Fe_3O_4@OA, (b) Fe_3O_4@CTA, (c) Fe_3O_4@PEGMA, (d) Fe_3O_4@PEGMA-pMAL3, (e) Fe_3O_4@PEGMA@N_3-3 and (f) Fe_3O_4@PEGMA-MAL3 49

LIST OF TABLES

Table 1.1. Comparison of synthetic methods to produce magnetic NPs [8]. 2
Table 4.1. End groups maleimide modified NPs according to AIBN/Maleimide ratio before and after retro Diels-Alder reaction. 37
Table 4.2. End groups azido modified NPs according to AIBN/Azido ratio. 41

1. INTRODUCTION

1.1. Iron Oxide Nanoparticles

Iron oxide nanoparticles (NPs) have attracted much attention due to their potential applications in hyperthermia [1], drug delivery [2], magnetic resonance imaging (MRI) contrast agent, magnetic cell labelling [3] and cell separation [4]. Narrow size distribution of nanoparticles is important to ensure that each individual NP has the same physical and chemical properties for these applications [5]. In addition, the performance and magnetic properties of NPs are mainly determined by their dimension [6]. The stability of magnetic NPs under different conditions is another crucial requirement for successful application in biomedicine. Consequently, several routes such as thermal decomposition, co-precipitation and microemulsion have been developed to produce stable and highly monodisperse NPs.

Surface coating plays an important role since iron oxide NPs easily form large clusters because of their high surface area to volume ratio [7]. Besides, non-coated magnetic nanoparticles can easily undergo oxidation in air. Because of that, surface coating of nanoparticles is of the utmost importance to decrease high surface energy [8] and prevent their agglomeration. Magnetic NPs are mainly stabilized by hydrophobic or hydrophilic dispersants such as oleic acid, various polymers and inorganic materials [9]. The importance of surface coating comes from not only keeping down agglomeration arising from high surface energy but also by providing further functionality to magnetic NPs for various applications and more resistance towards biofouling under physiological conditions [10].

Two types of iron oxide NPs, namely magnetite (Fe_3O_4) and maghemite (γ-Fe_2O_3), have been investigated as promising candidates for biomedical applications owing to their biocompatibility [11] since they go into the body's iron metabolism as ferritin and/or hemosiderin [12]. The production of these two types of NPs has been examined thoroughly

for the last few decades, and procedures to obtain them large scale have been established [13].

1.1.1. Synthetic Pathway of Iron Oxide Nanoparticles

In recent years, several methods have been developed for producing monodisperse, shape-controlled and stable NPs. Conventional methods including thermal decomposition [14], microemulsion [15], co-precipitation [16], hydrothermal synthesis [17] and sonochemical synthesis [18] can be employed for the synthesis of high quality NPs. Co-precipitation and microemulsion methods are used for direct synthesis of water dispersible magnetic NPs while thermal decomposition procedure generally yields organic solvent dispersible NPs. However, the latter procedure provides more control over the size distribution and crystallinity [19]. Comparison of the synthetic methods is shown below in Table 1.1.

Table 1.1. Comparison of synthetic methods to produce magnetic NPs [8].

Synthetic method	**Synthesis**	**Reaction temp (°C)**	**Reaction period**	**Solvent**	**Surface capping-agents**	**Size distribution**	**Shape control**	**Yield**
Co-precipitation	very simple, ambient conditions	20-90	minutes	water	needed, added during or after reaction	Relatively narrow	Not good	High / scalable
thermal decomposition	complicated, inert atmosphere	100–320	hours–days	organic compound	needed, added during reaction	very narrow	very good	high/ scalable
microemulsion	complicated, ambient conditions	20–50	hours	organic compound	needed, added during reaction	relatively narrow	good	low
hydrothermal synthesis	simple, high pressure	220	hours ca. days	water-ethanol	needed, added during reaction	very narrow	very good	medium

Co-precipitation method is widely used owing to the fact that it requires mild reaction conditions compared with the other methods, such as low reaction temperature and time. Fe_3O_4 and γ-Fe_2O_3 are synthesized by mixing ferric and ferrous salts (in 1:2 molar

ratio) with a strong base in co-precipitation method. The chemical reaction that occurs during iron oxide NP formation is given as follows:

$$Fe^{2+} + 2Fe^{3+} + 8OH^{-} \longrightarrow Fe_3O_4 + 4H_2O$$

$$Fe_3O_4 + 2H^{+} \longrightarrow Fe_2O_3 + Fe^{2+} + H_2O$$

In the first step, magnetite (Fe_3O_4) NPs are obtained at pH between 8 and 14 but magnetite is sensitive to air and forms maghemite (γ-Fe_2O_3) by oxidation when it is exposed to air [7]. Beside difficult control over the process, it is not fully known the influence of synthetic parameters such as pH value, temperature and stirring rate [20]. Furthermore, the size distribution of NPs is in a wide range and secondary size selection is needed [11, 21].

In thermal decomposition procedure, different precursors of iron like $Fe(CO)_5$ [22], $Fe(acac)_3$ [23] and iron oleates [24] decompose at high temperature in a high boiling point solvent to give monodisperse iron oxide NPs. Size and shape of NPs depend on various factors such as heating rate, boiling point of the solvent and the surfactant. The most common surfactant used in thermal decomposition process is oleic acid.

1.1.1.1. Thermal Decomposition Procedure. Thermal decomposition of different iron precursors is widely used to produce highly monodisperse magnetic NPs in a large scale. The quality of NPs is determined by different factors such as heating rate, refluxing time and so on. The effects of reaction temperature, surfactant concentration, seed-mediated growth, reaction concentration and heating rate on the size of iron oxide NPs were examined by Chen [25]. Iron oleate complex was utilized as iron precursor for the synthesis of iron oxide NPs. 1-octadecene (~320 ^{o}C), eicosane (~360 ^{o}C) and docosane (~380 ^{o}C) were used as solvents to investigate the effects of reaction temperature on iron oxide NPs. Sizes of NPs were 12.5 nm, 17.6 nm and 22.5 nm after refluxing at 320 ^{o}C, 360 ^{o}C and 380 ^{o}C, respectively (Figure 1.1). Moreover, it was depicted that the refluxing time affected the shape of NPs from spherical to cubic with prolonged time; while there was no effect on the size of NPs.

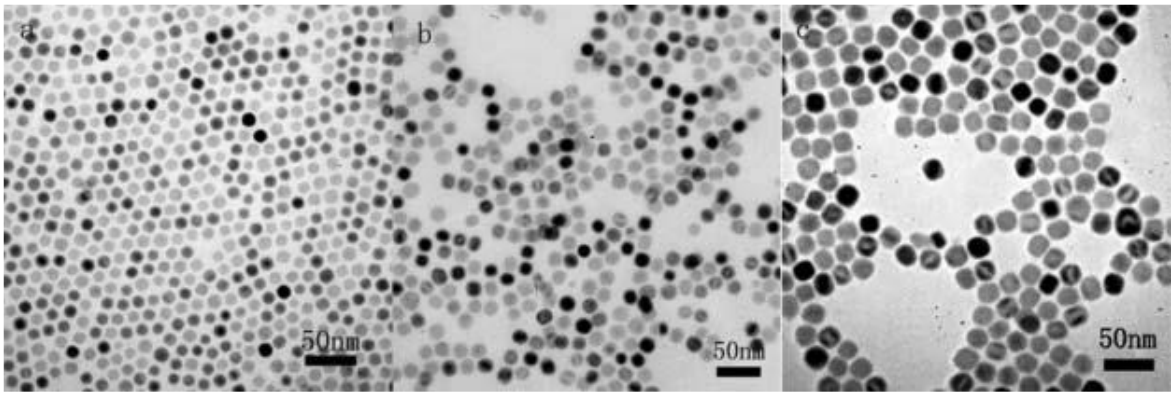

Figure 1.1. TEM images of a) 12.5 nm b) 17.6 nm and c) 22.5 nm iron oxide nanoparticles using octadecene, eicosane and docosane as solvents, respectively [25].

Hyeon *et al*. proposed a mechanism for the nanocrystal formation using iron oleate precursor [24]. Nucleation takes place by dissociation of one oleate with CO_2 elimination from iron oleate complex at 200-240 ^oC. Two oleate ligands start dissociating from iron at ~300 ^oC, which is the major growth of NPs. Finally, monodisperse NPs are obtained from separation of nucleation and growth process.

Thermal decomposition procedure allows more control over produced NPs by arranging temperature, refluxing time, heating rate and so on. Ultra-large scale synthesis of magnetic NPs has been already examined by Hyeon *et al*. [24] and it is now possible to get iron oxide NPs in a large scale using non-toxic and inexpensive reactants.

1.2. Surface Modification of Iron Oxide Nanoparticles

Naked NPs tend to agglomerate and from large clusters, which brings about increased particle size. Additionally, these clusters show ferromagnetic behavior springing from strong magnetic dipole-dipole attractions [26]. Hence, surface modification of magnetic NPs is very important for many applications. Magnetic NPs can be easily coated with different organic or inorganic groups in order to increase their stability in various environment. Suitable anchoring groups are needed to graft polymers or inorganic materials onto iron oxide NP

surface. The widely used anchoring groups for surface modification are dopamine [27], phosphonic acid [28], carboxylic acid [29], trimethoxy silane [30] and arsonic acid [31] since these groups show high affinity for iron oxide NP surface (Figure 1.2).

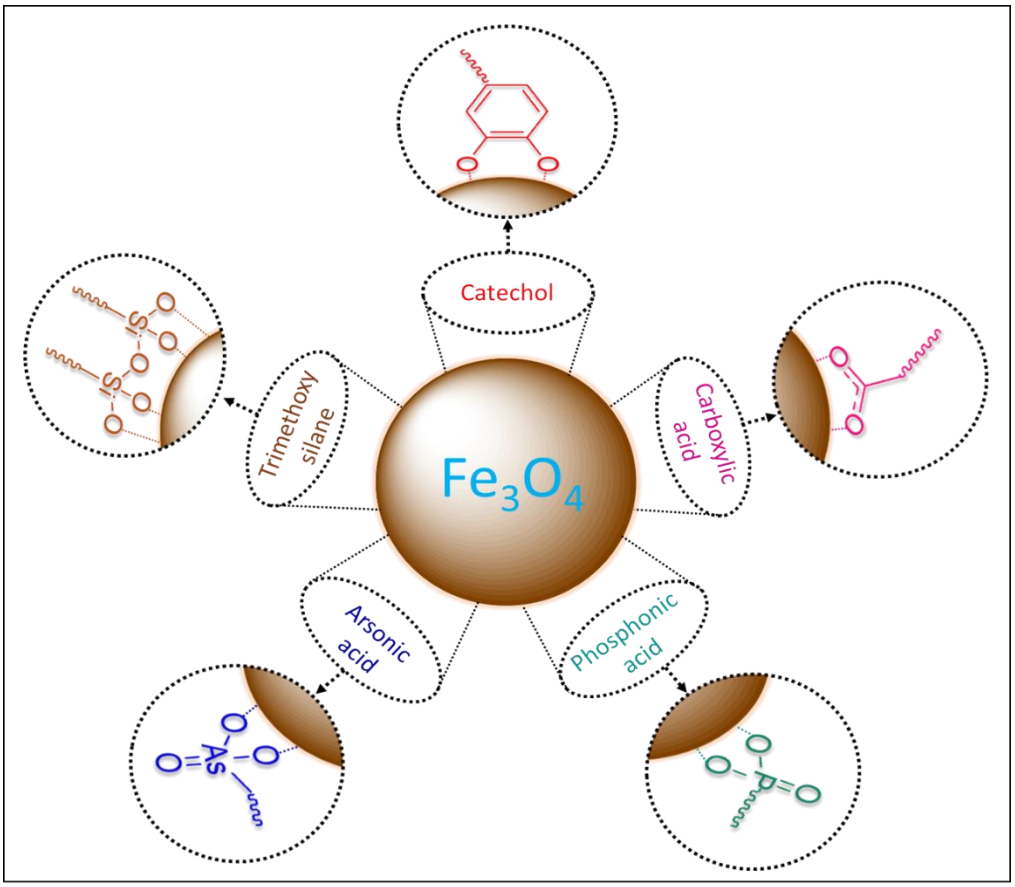

Figure 1.2. Most commonly used anchoring groups for iron oxide NPs.

1.2.1. Inorganic Materials

Inorganic materials such as silica, gold and gadolinium are used for surface modification of NPs for a long time in order to acquire functionality to iron oxide NPs and ensure good stability of these NPs, as well. For example, 3-aminopropyltriethoxysilane (APTES) is one of widely used coating material for getting amine functionality [32]. In addition, gold, having high affinity to thiol, is another inorganic coating material that can be used for bioapplications keeping physical properties of iron oxide NPs [33].

In the literature, there are many examples of silica coated iron oxide NPs. Silica has ample silanol groups on silica layer, and this groups can be reacted with functional groups such as amines, thiols and carboxylic acids, etc. [34]. Additionally, it enhances iron oxide NPs' hydrophilicity, biocompatibility and colloidal stability and it is optically transparent, as well [35, 36]. Earhart *et al*. showed conjugation of carbohydrate to silica coated iron oxide NPs [37] because carbohydrate functionalized NPs are important for investigating glycobiological events. They used dextran as carbohydrate and successfully conjugated with amine functionalized silica coated NPs (Figure 1.3).

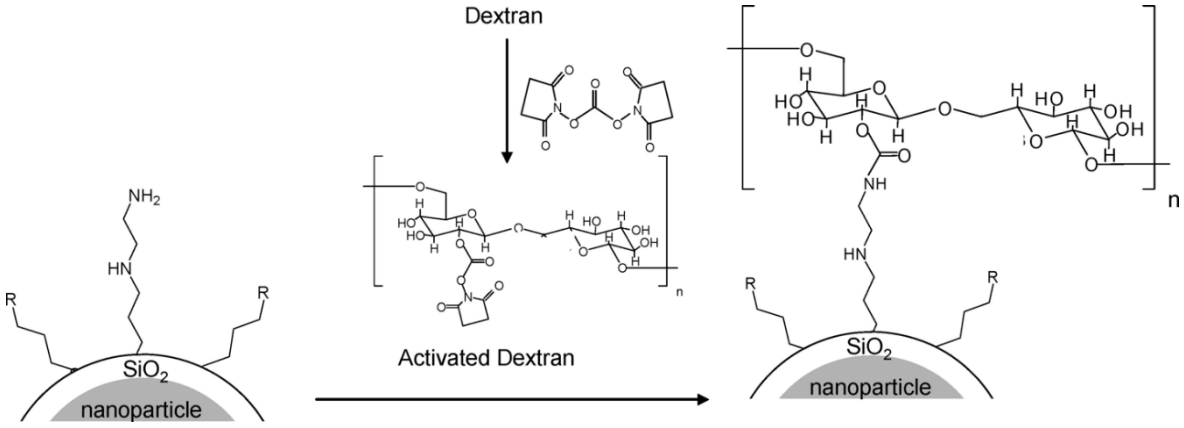

Figure 1.3. Dextran conjugation to amine functionalized silica coated NPs [37].

Another way to modify magnetic NP surface is to investigate metal or non-metal shell. Gold is a promising candidate for stabilization and further functionalization of iron oxide NPs. Gold coated NPs have a wide range of biomedical application owing to their biocompatibility, chemical stability and easy thiol modification [38].

1.2.2. Organic Materials (Polymers)

Polymer used for surface modification of iron oxide NPs are divided into two categories, natural and synthetic polymers. Dextran [39], starch [40], gelatin [41] and

chitosan [42] are the most common natural organic modifiers for iron oxide NPs. These organic materials are exploited the potential biomedical applications. For example, Gaihre *et al*. worked on drug loading and *in vitro* drug release study of gelatin coated iron oxide NPs. They used doxorubicin that is anthracycline antineoplastic agent for their study, and indicated drug loading capacity of iron oxide NPs by charged-induced adsorption. Also, they examined drug release profile by changing the pH from 4 to 7.4 [41].

Synthetic polymer modification of iron oxide NPs has recently become one of the most investigated areas. Different polymers like poly(2-(dimethylamino)ethyl methacrylate) [43], poly(N-isopropylacrylamide) [44], poly(PEGMA) [45], polystyrene [30] and poly(N-hydroxysuccinimide) [46] were grafted onto iron oxide surface for various applications. Functionalization of NPs with different polymers could provide combined advantages [29]. For example, polyethylene glycol (PEG) is used to afford NPs biocompatibility and good water solubility while physical properties of NPs are still maintained [45, 47].

The efficient two approaches for polymer coating of NPs are grafting-to and grafting-from methods [48, 49]. The detailed mechanisms of these two approaches is given in the next section below.

1.2.2.1. Grafting-to Approach. In this method, polymers bind to iron oxide NP surface with suitable anchoring groups, electrostatic attraction or hydrophobic interactions [50]. However, the grafting density of NPs is low owing to steric hindrance of polymers that are already anchored to the surface (Figure 1.4). Surface grafting density is determined by the molecular weight of polymers. Increase of the molecular weight gives rise to increase in steric hindrance, and decrease in grafting density, as expected [51]. Despite low grafting density, this approach allows more control over polymer architecture and characterization.

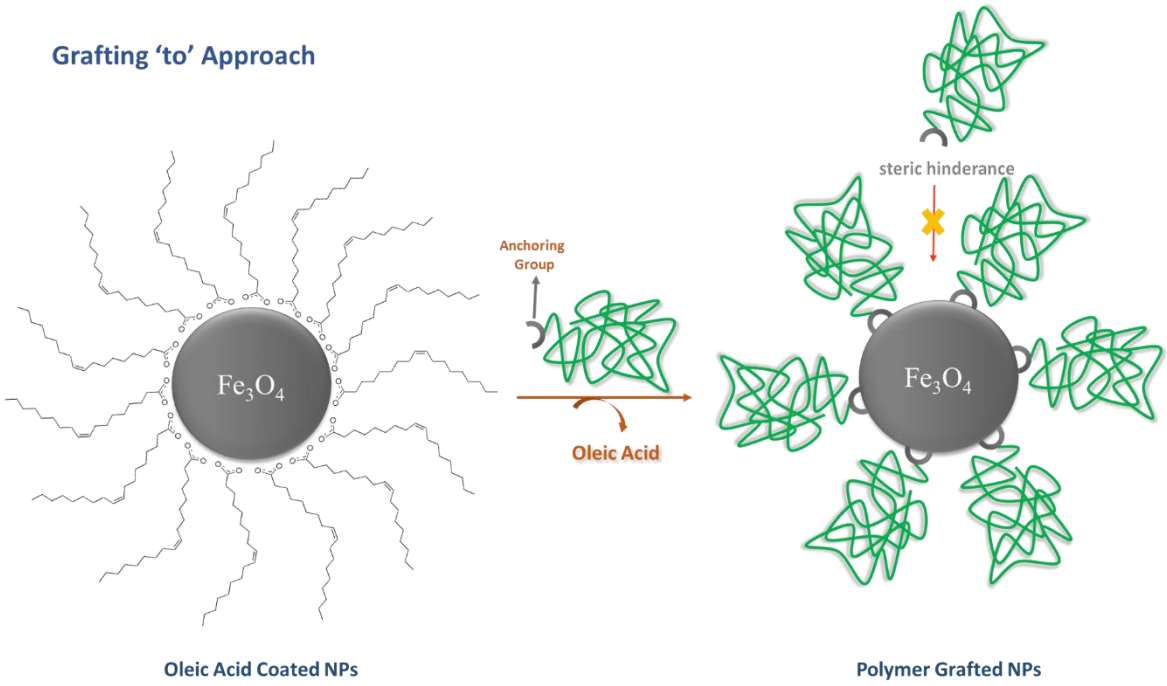

Figure 1.4. Polymer conjugation to iron oxide NP by grafting-to method.

Mattoussi *et al*. synthesized multidentate catechol-based polyethylene glycol oligomers [52]. After synthesis of the oligomers, they immobilized these well-defined catechol and functional groups containing oligomers to the surface of iron oxide NPs by means of powerful catechol-iron affinity. Synthesis of oligomers was indicated in Figure 1.5.

In this example, the polymer was functionalized with azide group and bound to iron oxide surface by catechol groups. Then, azide functionalized OligoPEG-Dopa-NPs were reacted with alkyne modified rhodamine B dye in order to show efficient azide-alkyne cycloaddition (CuAAC).

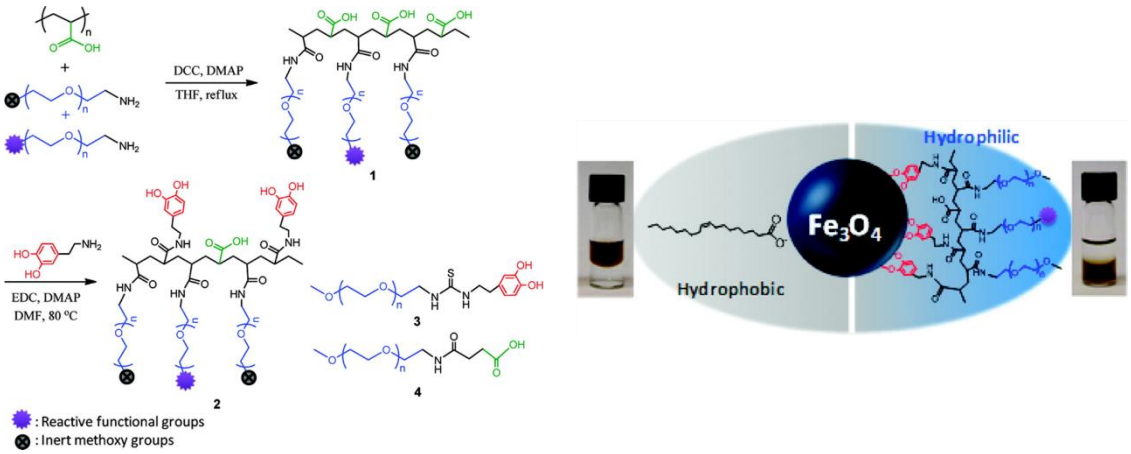

Figure 1.5. Preparation of the carboxyl- and catechol-PEG-derivatized oligomers and immobilization onto iron oxide NP surface [52].

1.2.2.2. Grafting-from Approach. Another efficient way for NP surface modification is to grow desired polymers from the surface, which is called grafting-from method. Grafting-from approach has been studied using wide range of polymerization techniques, which are atom transfer radical polymerization (ATRP) [53], ring opening polymerization ROP [54], reversible addition-fragmentation chain transfer polymerization (RAFT) [55] and nitroxide mediated radical polymerization (NMP) [47]. Compared to grafting-to approach, higher grafting density can be achieved by grafting-from method that enhances the stability of NPs [51]. Furthermore, a brush-like polymer coatings are obtained by grafting-from methodology.

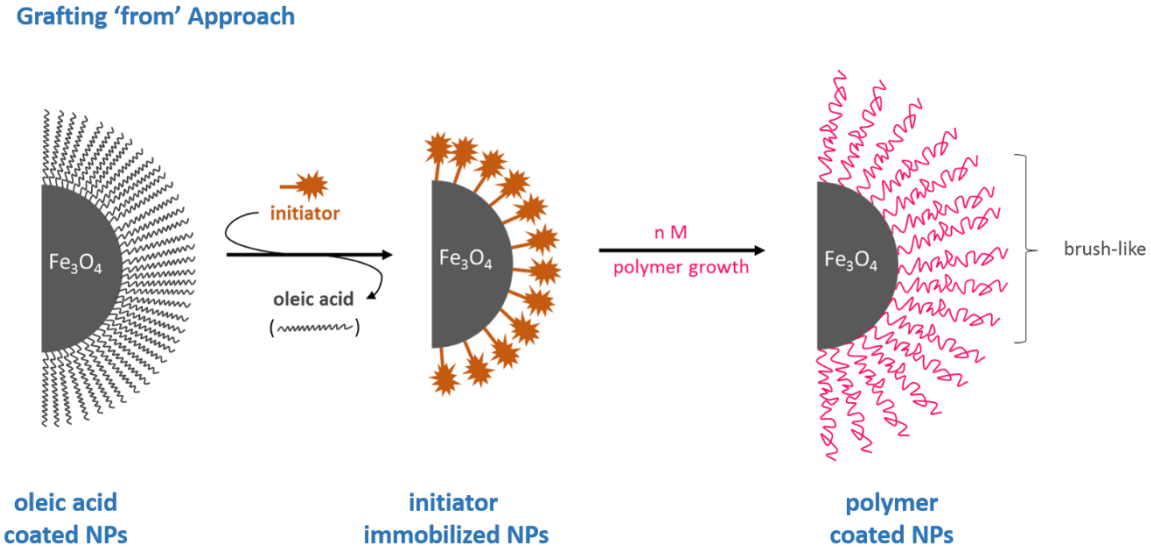

Figure 1.6. Polymer conjugation to iron oxide NP by grafting-from method.

The first step of grafting-from approach is anchoring suitable initiators to NP surface, and then growing polymers directly from the surface (Figure 1.6). It is possible to control thickness by reaction time and concentration of monomer, and grafting density by tuning initiator density [9]. Yuan *et al.* [29] used this method to produce p(2-hydroxyethyl methacrylate)-graft-p(ε-caprolactone) coated NPs by utilizing both ATRP and ROP (Figure 1.7).

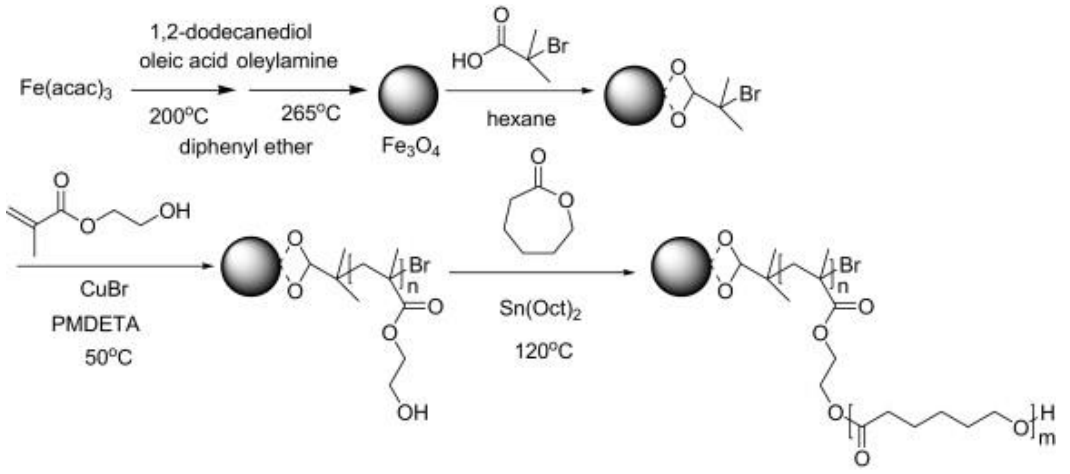

Figure 1.7. Synthesis of Fe_3O_4@PHEMA-g-PCL magnetic NPs by ATRP and ROP [29].

The ATRP initiator was immobilized onto iron oxide NP surface via carboxylic acid group, and 2-hydroxyethyl methacrylate (HEMA) monomer was polymerized with surface initiated atom transfer radical polymerization (SI-ATRP). Biocompatible p(HEMA) have hydroxyl groups in the polymer's side chain, which could initiate a ring opening polymerization (ROP). Finally, the group achieved branched brush polymeric shells from iron oxide NP surface.

1.3. Reversible Addition-Fragmentation Chain Transfer (RAFT) Polymerization

As mentioned in previous section, polymer modification of iron oxide NPs by means of different monomers is an effective and important way for most applications. Various polymerization techniques such as atom transfer radical polymerization (ATRP) [56], nitroxide mediated radical polymerization (NMRP) [57] and reversible addition-fragmentation chain transfer polymerization (RAFT) [58] have been carried out modifying iron oxide NP surface. Even though ATRP has some advantages among these polymerization techniques, removal of copper based catalyst has been challenging and crucial for medical applications [59]. Likewise, NMRP requires high temperature and it can only be used for a limited number of monomers [60]. However, RAFT polymerization is suitable for a wide range of functional monomers compared to other polymerization techniques. Moreover, it enables easy end group modification of polymer brushes for further functionality [61, 62].

Chain transfer agents (CTA) are used in RAFT polymerization to control molecular weight distribution and ensure living characteristic of the polymerization. CTAs are thiocarbonylthio groups in which R group is a homolytic leaving group and Z is an activating group selected to alter reactivity of RAFT agent (Figure 1.8) [63]. It is of the utmost importance for successful polymerization to choose RAFT agent which is suitable for a particular monomer [64]. The general mechanism of RAFT polymerization is given in Figure 1.8. According to proposed mechanism, polymerization starts with decomposition of the initiator, and it follows propagation to give polymeric radical ($P_n\cdot$), which then reacts with CTA. Leaving group ($R\cdot$) departs with addition of $P_n\cdot$ to the CTA in the equilibrium step,

and it initiates another polymer chain. The equilibrium between propagating chains and RAFT agents determines how monodisperse polymers are obtained.

The formation of dead polymer chains are inevitable because of irreversible chain transfer in the termination step. Nevertheless, it is not as significant as compared with other conventional polymerization techniques since RAFT polymerization suppresses the formation of dead chains [65]. At the end of polymerization, most of the polymer chains keep the thiocarbonylthio end groups [66].

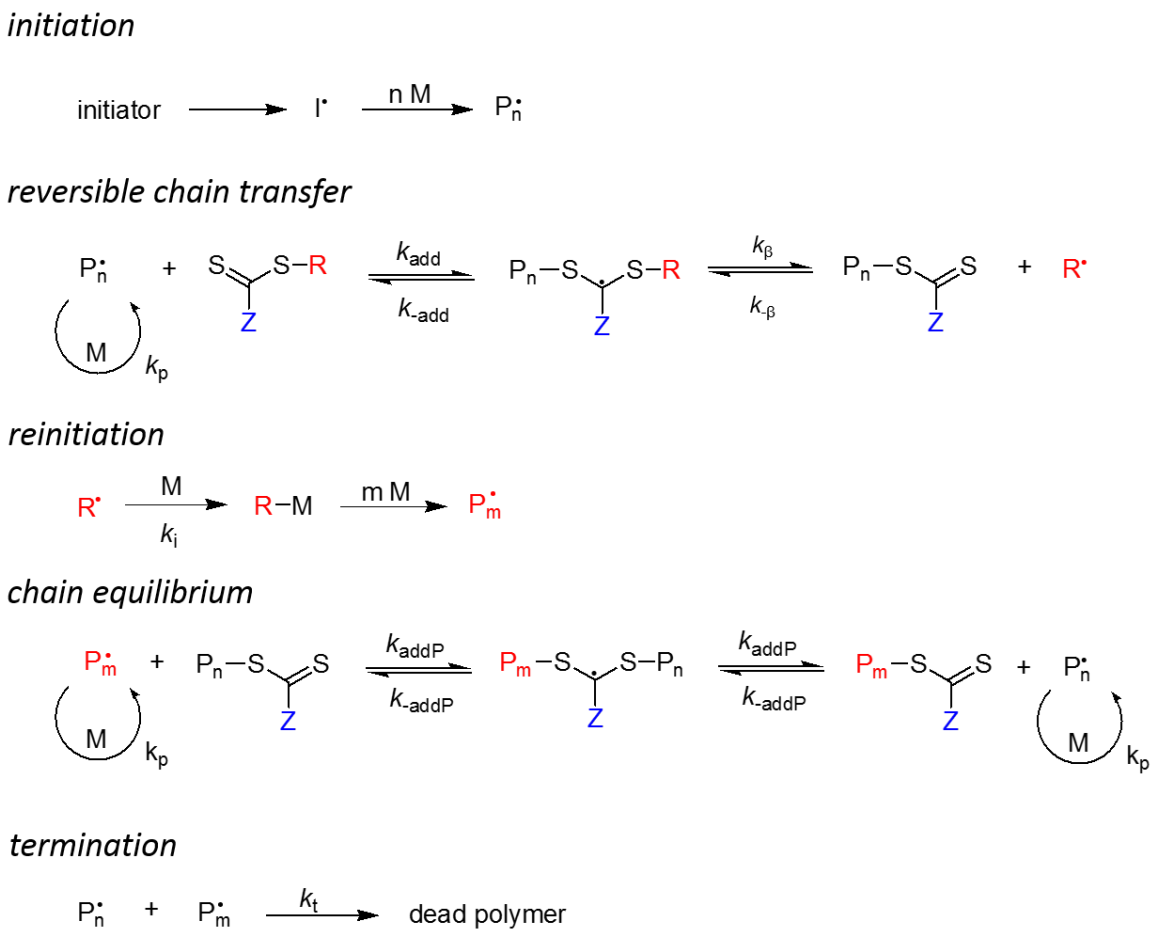

Figure 1.8. General mechanism of RAFT polymerization.

For successful RAFT polymerization, one must be careful choosing suitable RAFT agent, reaction conditions and monomer. Sustainability of the polymerization is achieved by precisely altering these conditions. For instance, styrenic and acrylic monomers can be effectively polymerized by using trithiocarbonates with an appropriate choice of R group, while xanthates are used for less activated vinyl monomers [67].

1.4. End Group Modification of RAFT Polymers

Post-polymerization modification method has been an effective way to introduce functionality into the ω-end of the polymer by means of different chemistries such as thermal elimination, nucleophile reactions (aminolysis, hydrolysis, ionic reduction) [68, 69] and radical coupling [70] (Figure 1.9). Besides acquiring ω-end functionality, modification of thiocarbonylthio groups is also important to decrease their intrinsic reactivity and prevent decomposition into fetid sulfur materials [71].

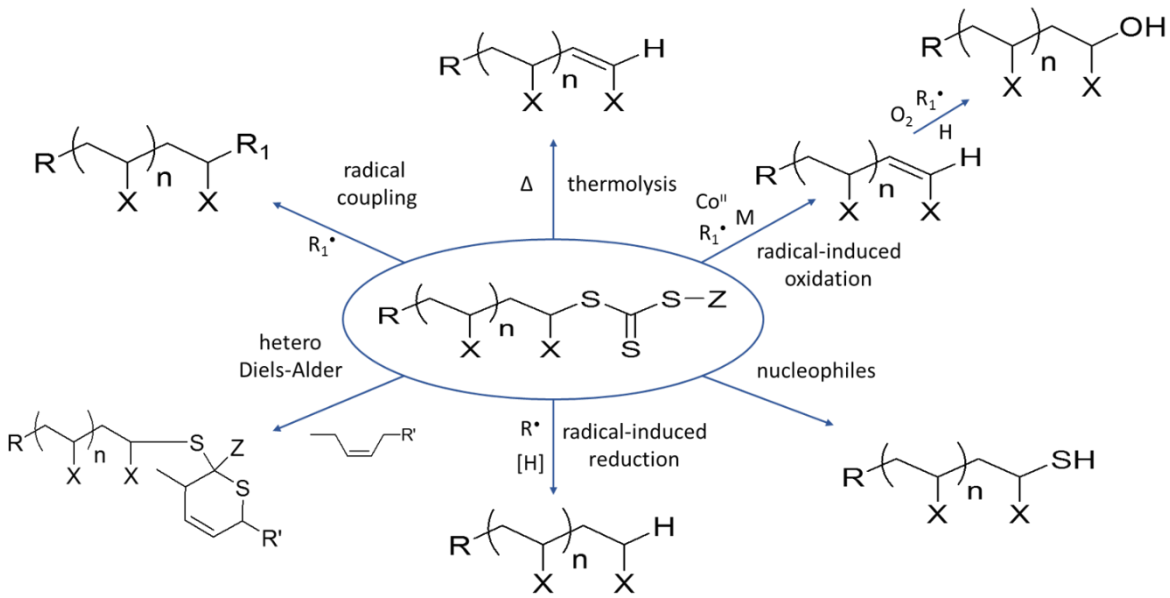

Figure 1.9. End group modification of RAFT polymer.

Radical coupling modification by heating RAFT polymer with an excess amount of a radical azo-initiator is now very popular for end group modification [72]. Maynard *et al.* [73] carried out radical coupling modification with protected maleimide containing azo-initiator for conjugation of two different proteins into RAFT polymer (Figure 1.10).

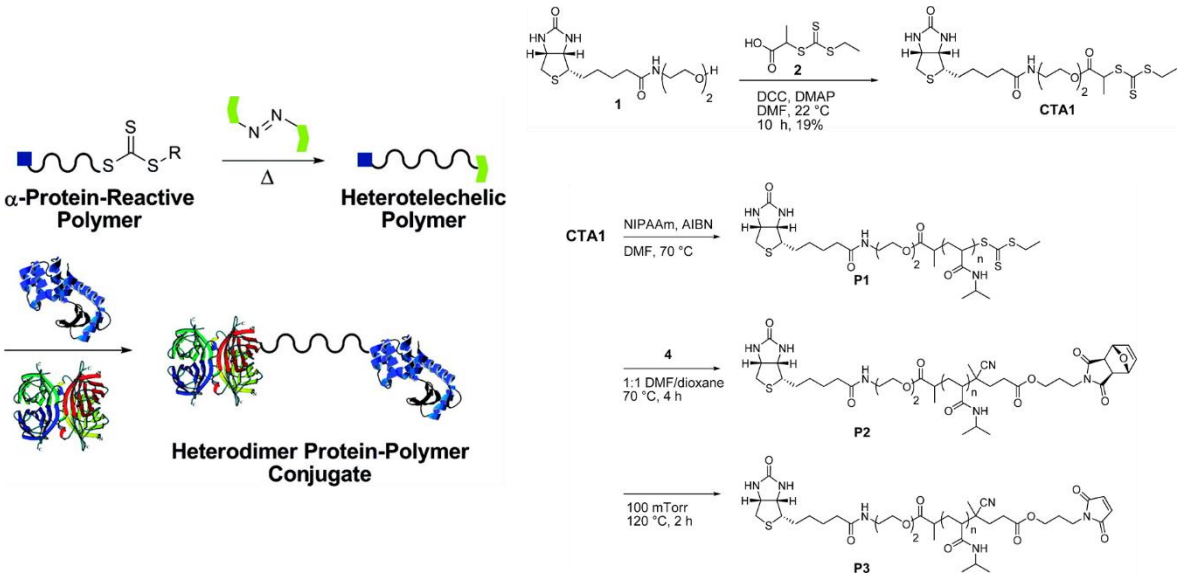

Figure 1.10. Synthesis of biotin-maleimide heterotelechelic pNIPAAm and conjugation of SAv and BSA [73].

The group synthesized α-biotinylated trithiocarbonate RAFT agent and carried out polymerization with this CTA using NIPAAm as monomer. This polymer was reacted with an excess amount of protected-maleimide groups containing azo-initiator via cross coupling reaction as shown in Figure 1.10. Biotin-maleimide telechelic polymer was easily conjugated with two different protein, streptavidin (SAv) and bovine serum albumin (BSA). Using this approach, different functional groups can be exploited according to desired application.

Nucleophile reactions (e.g. amines, hydroxides) have been used for end group modification of thiocarbonylthio based polymers. Thiocarbonylthio end groups are converted into thiol groups through reduction of thiocarbonylthio. Because of their efficiency under wide range of conditions, thiol based reactions have been employed in many

applications without side reactions [74]. Hexylamine [75], propylamine [76] and sodium borohydrate [77] are widely used nucleophiles for thiol end group modification of RAFT polymers. However, disulfide formation is one of the main challenge of this method, which requires a reagent to trap thiol [72]. Nonetheless, disulfide bonds can be broken by a subsequent reduction with tris(2-carboxyethyl)phosphine (TCEP) [71]. Additionally, use of hydrazine for end group modification revealed that it is very promising due to preventing disulfide formation to some extent and fast reduction of thiocarbonylthio groups [71].

1.5. Click Type Chemistry

Click type chemistry, a concept reported by Sharpless *et al*. in 2001 [78], is attractive due to its high yields, insensitivity to O_2, short reaction time, tolerance to solvent and functional groups and easy purification [79]. There are several types of click chemistry, and the most famous one is copper catalyzed 1,3-Huisgen dipolar cycloaddition reaction, also referred as copper catalyzed azide-alkyne click (CuAAC) [80]. Thiol-ene and thiol-yne are the other types of click reaction that are also widely utilized (Figure 1.11).

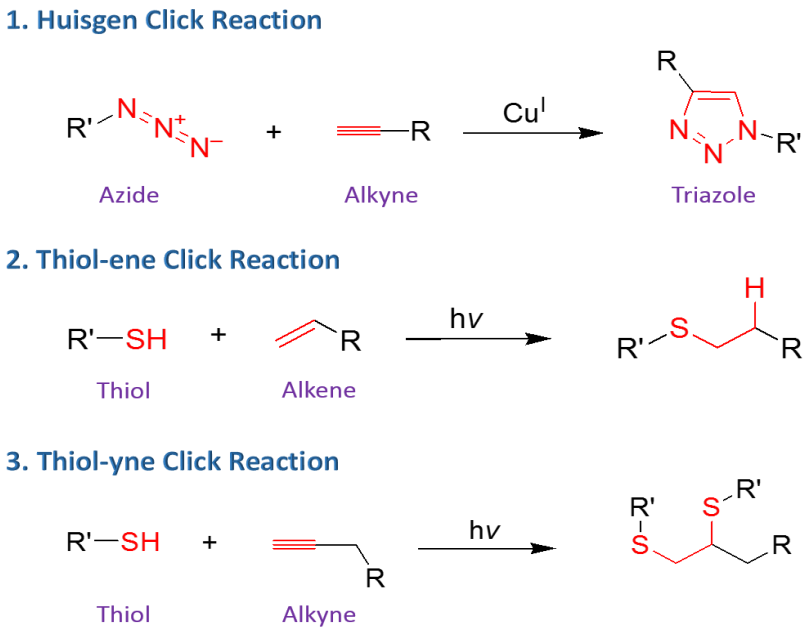

Figure 1.11. Commonly utilized 'Click' type reactions.

Click type reactions are also attractive owing to their orthogonality, which can be exploited for designing more complex architecture via CuAAC and thiol-ene click chemistry without hindering one another [81]. For instance, Yagci *et al*. synthesized a block co-polymer whereby CuAAC click chemistry and followed by conjugation of N-acetyl-L-cysteine (NAC) to alkene containing polymer via thiol-ene click chemistry in a one-pot. Biologically active block co-polymer PMMA-b-PCL-NAC was successfully obtained by one-pot sequential CuAAC and thiol-ene click chemistries (Figure 1.12).

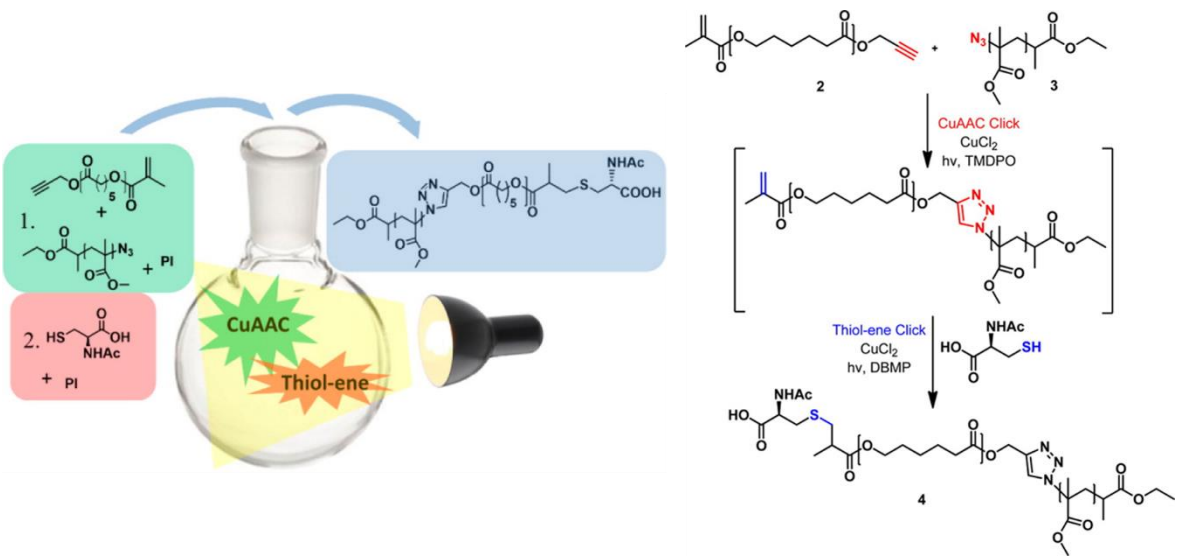

Figure 1.12. Sequential one-pot photoinduced CuAAC and thiol-ene click reactions yielding bio-active block co-polymer [81].

1.6. Maleimide-Thiol Michael Addition Reaction

Michael addition between maleimide and thiol groups is highly efficient and fast reaction in addition to its metal free nature. Maleimide-thiol based Michael addition reaction is commonly used bioconjugation of peptides or proteins [82]. Addition of thiol to maleimide is commenced by amines or phosphines with the deprotonation of thiol group. Especially, Michael addition of thiol takes place without any side reactions in the presence of triethylamine (TEA). The most efficient Michael reaction of thiol groups is achieved by

addition to electron deficient double bonds, and N-substituted maleimides with two electron withdrawing groups have been known to give the fastest Michael addition reaction [83].

One example of maleimide-thiol Michael addition reaction was carried out by Schirrmacher and Lennox *et al*. They used maleimide terminated polyethylene glycol (PEG) coated gold nanoparticles for *in vivo* applications (Figure 1.13) [84].

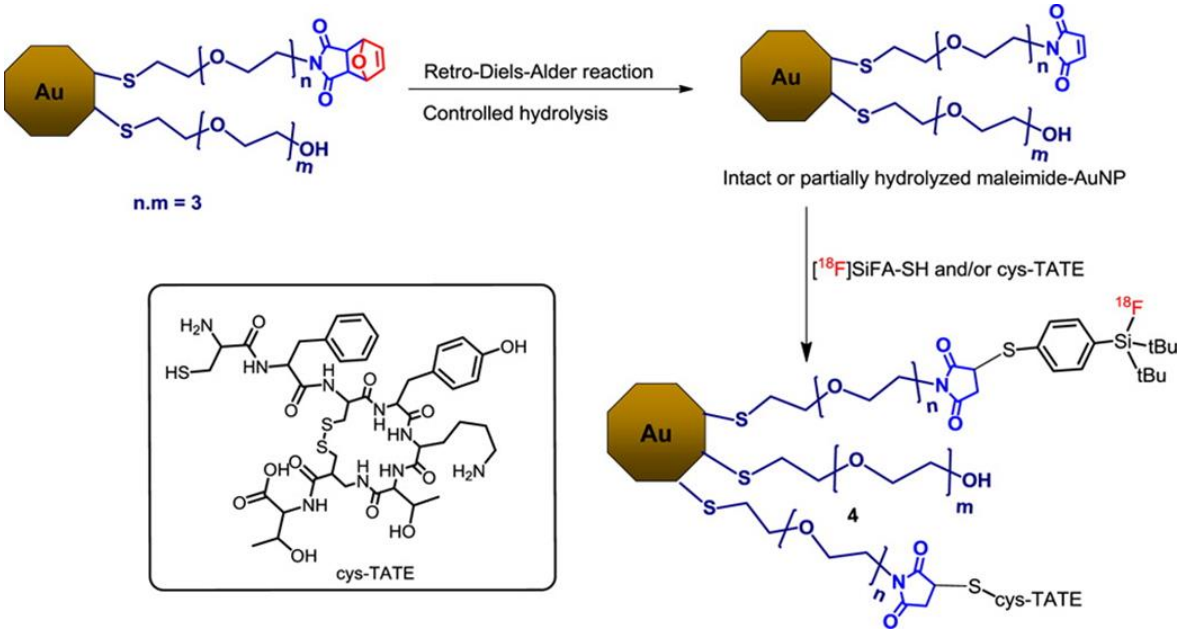

Figure 1.13. Reaction scheme of preparation of maleimide-Au NPs and Michael addition of SiFA-SH and cysteine derivative cys-TATE peptide [84].

Maleimide groups were conjugated with silicon−fluorine prosthetic group (SiFA) for radiolabelling and cysteine using maleimide-thiol chemistry. This conjugation brings about a promising protocol for derivation of gold or other nanoparticles with thiol bearing molecules.

2. AIM OF THE STUDY

Aim of this study is to produce water dispersible and reactive magnetic nanoparticles that can be used in biomedical applications. Polymer coating onto magnetic nanoparticle surface can be achieved by graft-from or graft-to methodology. Both requires suitable anchoring groups either at the end of the polymer or in the branching units of polymer chain in order to immobilize polymers onto nanoparticle surface.

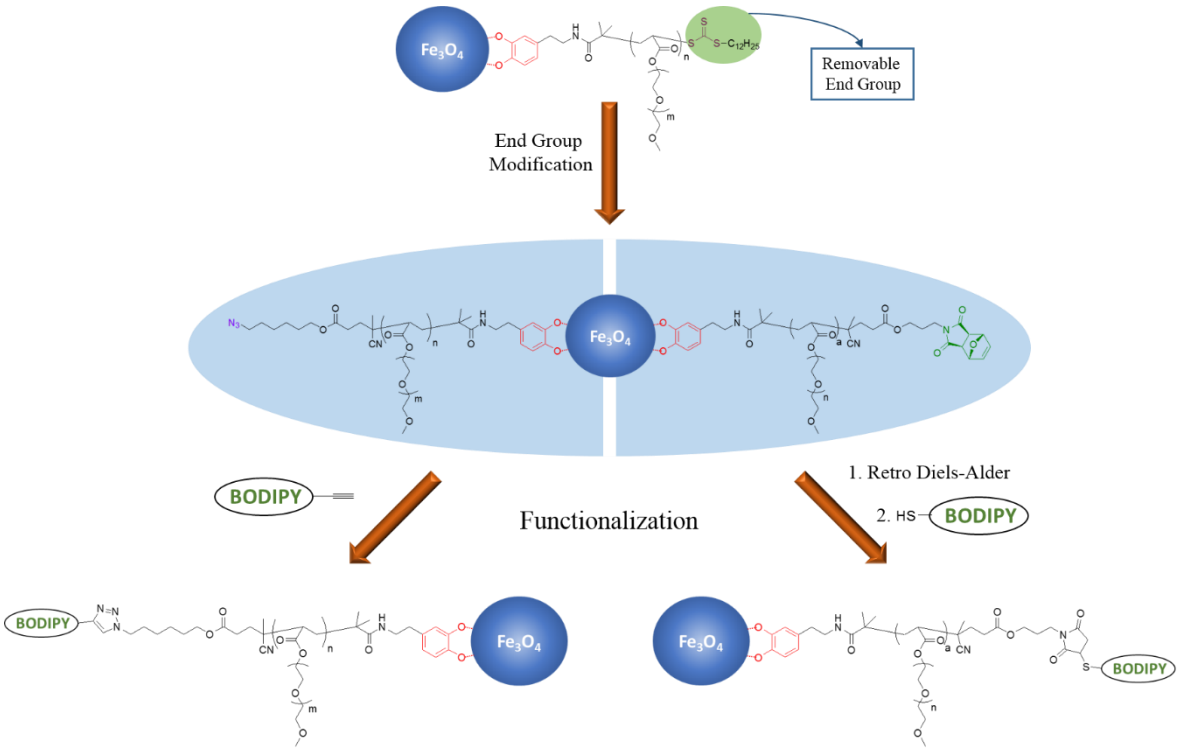

Figure 2.1. General scheme of the project

Catechol was used as an anchoring group for this study. After immobilization of catechol modified chain transfer agent onto iron oxide NPs, polymers were grown from the surface using RAFT polymerization in the presence of PEGMA monomer. Each iron oxide nanoparticle is surrounded by furan protected maleimide or azide groups by the reaction of

radical cross-coupling. The maleimide derivative of iron oxide nanoparticles can be generated through a retro Diels-Alder reaction. Functionalized nanoparticles can be reacted with thiol containing molecules by Michael addition. Likewise, azide functionalized nanoparticles can be reacted with alkyne bearing compound by Huisgen azide-alkyne click reaction. The successful conjugation with thiol and alkyne bearing compounds can be investigated via the attachment of a fluorescent dye.

3. EXPERIMENTAL

3.1. Materials

Iron (III) chloride hexahydrate ($FeCl_3.6H_2O$), oleic acid, 1-dodecanethiol, aliquot® 336, dopamine hydrochloride, triethylamine (TEA), thionyl chloride and 4-(dimethylamino) pyridine (DMAP) were purchased from Sigma-Aldrich and used without further purification. Poly(ethylene glycol) methyl ether acrylate (PEGMEA, number-average molecular weight M_n = 480) was purchased from Sigma-Aldrich and purified over basic aluminum oxide before use. 2,2'-azobis(2-methylpropionitrile) (AIBN, Sigma) was recrystallized from ethanol. 1-octadecene, N-Hydroxysuccinimide (NHS), 1-(3-dimethylaminopropyl)-3-ethylcarbodiimide hydrochloride (EDCI) were purchased from Alfa-Aesar. Sodium oleate was purchased from TCI. Carbon disulfide (CS_2), 4,4'-azobis(4-cyanovaleric acid) (V501) were purchased from Fluka. Column chromatography was performed using silica gel 60 (43-60 nm, Merck). Thin layer chromatography was performed using silica gel plates (Kieselgel 60 F254, 0.2 mm, Merck). Furan protected maleimide containing alcohol (2) [85], BODIPY thiol [86] and alkyne [87], 6-azido-1-hexanol [88] and protected maleimide V501 derivative (3) [73] were synthesized according to previous literature examples. 2-(Dodecylthiocarbonothioylthio)-2-methyl propionic acid (DDMAT) was synthesized according to Lai *et al*. [89]. Dichloromethane (DCM), ethanol, chloroform, dimethylformamide (DMF), n-hexane, toluene and 1,4-dioxane were purchased from Merck. Anhydrous toluene, tetrahydrofuran (THF) and dichloromethane (DCM) were taken from SciMatCo purification system, and other anhydrous solvents were dried over molecular sieves.

3.2. Measurements

Dynamic Light Scattering (DLS) measurements were done in DMF and hexane at 20 ^oC on a Malvern Zetasizer Nano ZS photometer. Elemental analysis was performed by a Thermo Electron S.p.A. Flash EA® 1112 elemental analyzer. Transmission electron

microscopic (TEM) observation was carried out on LVEM5 microscope operated at 5 kV. Thermal gravimetric analysis (TGA) was conducted on a TA instruments heating rate 10 ^{o}C/min under a nitrogen atmosphere. Fourier transform infrared spectroscopy (FT-IR) was done on Thermo Fisher Scientific Inc.; Nicolet 380. ^{1}H NMR and ^{13}C NMR spectra were obtained on a Varian 400 MHz.

3.3. Synthesis of Iron Oxide Nanoparticles

3.3.1. Synthesis of Iron Oleate Complex

Iron oleate complex was synthesized according to previous report [24]. Iron chloride ($FeCl_3.6H_2O$, 2.56 g, 9.5 mmol) and sodium oleate (8.66 g, 28.5 mmol) were dissolved in a mixture of 19 ml ethanol, 14 ml distilled water and 33 ml hexane. The mixture was heated up to 70 ^{o}C and kept at that temperature for four hours. Organic layer which contains iron oleate complex was washed with distilled water in a separatory funnel. This cleaning process was repeated three times, and excess hexane was removed via rotary evaporation. Iron oleate complex was obtained in a waxy solid form.

3.3.2. Iron Oxide Nanoparticles by Thermal Decomposition Method

Monodisperse iron oxide nanoparticles were synthesized according to reported articles [24, 90]. 11 mmol iron oleate complex and 5.6 mmol oleic acid was dissolved in 71 ml of 1-octadecene by stirring vigorously. The mixture was heated up to 110 ^{o}C and kept at that temperature for 15 min in order to remove moisture. After 15 minutes, the mixture was heated to 320 ^{o}C with heating rate 3 - 4 ^{o}C/min and kept at that temperature for 30 min. Then, the resulting nanoparticles were cooled to room temperature before residual removal. Nanoparticles were precipitated from ethanol and collected by centrifugation. This process was repeated at least three times. Finally, the nanoparticles dispersed in hexane were again precipitated from acetone to get rid of all 1-octadecene residual and kept in hexane for further reactions after collecting by centrifugation.

3.4. Preparation of Catechol Modified Chain Transfer Agent

3.4.1. Synthesis of 2-(Dodecylthiocarbonothioylthio)-2-methylpropanoic acid (DDMAT)

The synthetic route of DDMAT was taken from literature [89]. Briefly, 1-dodecanethiol (3.7 g, 18.3 mmol), acetone (10.7 g, 184.2 mmol) and Aliquot336 (0.299 g, 0.74 mmol) were mixed in a round bottom flask and cooled to 10 ^{o}C under nitrogen atmosphere. After dropwise addition of 1.55 g of sodium hydroxide solution (50 wt %) over 20 min, it was stirred for an additional 20 min. Carbon disulfide (1.4 g, 18.4 mmol) and acetone (1.86 g, 32.0 mmol) mixture was added dropwise over 20 min. Before chloroform (3.28 g, 27.5 mmol) was added in one portion, the mixture was stirred for 10 min. Then, 7.37 g of sodium hydroxide solution (50 wt %) was added dropwise over 30 min, and 0.92 g of sodium hydroxide solid was added to the reaction mixture. Resulting mixture was stirred overnight. 30 ml of water and 5 ml of concentrated HCl was added to the reaction mixture, respectively. Yellow solid was collected by filtration and redispersed in 30 ml of methanol for 10 min in order to filter undissolved residuals off. The filtrate was dried by rotary evaporation and redispersed in 20 ml of methanol to remove trace impurity. To obtain pure DDMAT, solid was recrystallized from 35 ml of hexane (2.3 g, 40.4% yield).

3.4.2. Synthesis of DDMAT Succinimide (DDMAT-NHS) Ester

Succinimide ester of RAFT agent was synthesized previously reported article [91]. DDMAT (1.0 g, 2.75 mmol) and NHS (0.35 g, 3.0 mmol) were mixed and dissolved in dry DMF (14 ml). Then, EDC (0.57 g, 3 mmol) was added to the reaction mixture and stirred at room temperature for 24 h. DMF was evaporated via rotary evaporation. Yellow solid was purified washing by methanol several times, and dried under vacuum to obtain DDMAT-NHS ester (0.95 g, 75% yield).

3.4.3. Synthesis of Dopamine Terminated Chain Transfer Agent (Dopa-CTA)

Dopamine.HCl (0.3 g, 2.28 mmol) was dissolved in DMF (10 ml), and TEA (0.23g, 2.28 mmol) was slowly added to this solution by stirring for 15 min. Then, DDMAT-NHS ester (0.952 g, 2.06 mmol) was added to the solution. After 24 h stirring under darkness, the reaction mixture was dripped into an aqueous phosphate solution (60 ml, pH 4.0) to obtain yellow precipitate. The precipitate was collected by filtration and dried by lyophilizer. The product was then purified by column chromatography using chloroform/ethyl acetate (1:1) (0.9 g, 88% yield). ^{1}H NMR ($CDCl_3$) δ (ppm): 6.79 (d, 1H, C-C*H*=C-OH), 6.68 (d, 1H, C=C*H*-CH), 6.56 (dd, 1H, CH-C*H*=C-OH), 5.64 (s, 1H, N*H*), 3.44 (dd, 2H, NH-CH_2-CH_2), 3.25 (dd, 2H, NH-CH_2-CH_2-C), 2.66 (t, 2H, S=C-S-CH_2), 1.71 – 1.57 (m, 8H, S-C-(CH_3)$_2$-C=O, S-CH_2-CH_2-$(CH_2)_9$-CH_3), 1.43 – 1.19 (m, 18H, CH_2-(CH_2)$_9$-CH_3), 0.88 (t, 3H, CH_2-$(CH_2)_9$-CH_3). ^{13}C NMR ($CDCl_3$) δ (ppm): 219.8, 173.3, 144.1, 142.9, 130.6, 120.6, 115.2, 57.0, 41.7, 37.2, 34.5, 31.9, 29.6, 29.5, 29.4, 29.3, 29.1, 29.0, 27.7, 25.8, 22.7, 14.1. Anal Calcd. [$C_{25}H_{41}NO_3S_3$]: C, 60.08; H, 8.27; N, 2.80; S, 19.24. Found: C, 59.51; H, 8.55; N, 2.84; S, 20.24.

3.5. Synthesis of 4,4’-azobis(azidohexanoyl 4-cyanopentanoate)

4,4’-azobis(4-cyanovaleric acid) (V-501) (1 g, 3,6 mmol), 6-azido-1-hexanol [88] (1.33 g, 9.3 mmol), DMAP (174 mg, 1.4 mmol) and EDC (1.5 g, 7.8 mmol) were dissolved in 10 ml of dry DCM at room temperature. After reaction mixture was stirred for 24 h, the mixture was extracted with $NaHCO_3$, and dried over sodium sulfate ($NaSO_4$). Then, the solvent was removed by rotary evaporation, and diazido-V-501 (1) was purified by column chromatography with ethyl acetate/hexane (1:4) (0.92g, 48% yield). ^{1}H NMR ($CDCl_3$) δ (ppm): 4.11 (m, 4H, COOCH_2), 3.37 (t, 4H, N_3CH_2), 2.58 – 2.30 (m, 8H, CO-CH_2CH_2-C), 1.73 (s, 3H, CH_3), 1.70 – 1.53 (m, 11H, C-CH_2CH_2-C, CH_3), 1.48 – 1.32 (m, 8H, C-CH_2CH_2-C). ^{13}C NMR ($CDCl_3$) δ (ppm): 171.3, 117.5, 71.8, 65.0, 51.3, 33.2, 29.1, 28.7, 26.3, 25.5, and 24.0. Anal Calcd. [$C_{24}H_{38}N_{10}O_4$]: C, 54.36; H, 7.17; N, 26.41. Found: C, 54.81; H, 7.92; N, 25.78.

3.6. Synthesis of 4-(3-Hydroxypropyl)-10-oxa-4-azatricyclo[5,2,1,0]dec-8-ene-3,5-dione

The synthesis of maleimide derivative of V-501 (3) was synthesized according to previous literature example [73]. Briefly, V-501 (2.54 g, 9.1 mmol) and thionyl chloride (16.38 mg, 137.1 mmol) were dissolved in a mixture solvent of DMF and ethyl acetate (0.05:20 ml, respectively) under nitrogen protection. Then, the mixture was heated to 60 ^{o}C and waited until turning clear (~10 min). The temperature was kept at 60 ^{o}C for additional 20 min. and then cooled to 23 ^{o}C. After removal of the solvent, a yellow solid which is the acid chloride derivative of V-501 was used in the next step without further purification.

Compound **2** (2.90 g, 13.0 mmol) and Et_3N (1.41 g, 13.9 mmol) were dissolved in dry THF (50 ml) and stirred under nitrogen protection in an ice-water bath for 20 min. Acid chloride derivative of V-501 (1.59 g, 5.0 mmol) was dissolved in THF (20 ml) and added to the mixture dropwise over 20 min. After addition of acid chloride, ice-water bath was removed and the reaction was kept at room temperature for 4 h. Then, the solid was filtered off and THF was removed by rotary evaporation. The product **3** was purified by column chromatography using ethyl acetate/hexane (7:3 to 100 % ethyl acetate) (1.59 g, 48% yield).

3.7. Ligand Exchange Procedure

General procedure for ligand exchange was carried out according to the literature example [92] with some modifications. Oleic acid stabilized iron oxide NPs (50 mg) were dissolved in 5 ml of chloroform, and Dopa-CTA (250 mg) was added to the solution. The mixture was stirred at 40 ^{o}C for 48 h under nitrogen protection. Then, the reaction mixture was concentrated by rotary evaporation. Methanol was added to the mixture. Precipitated magnetic NPs were collected by a permanent magnet, and redispersed in THF. The precipitation process was repeated until all ungrafted DOPA-CTA was removed.

3.8. Surface-Initiated RAFT Polymerization of PEGMA

Dopa-CTA anchored NPs (25 mg), PEGMA (1.6 g, 3.3 mmol) and AIBN (2.2 mg, 13.4 μmol) were mixed in 3 ml of toluene, and purged with nitrogen for 20 min. The reaction mixture was put in a preheated oil bath at 70 ^{o}C for 24 h. After polymerization, polymer coated NPs were precipitated from the mixture of THF/Ether (1:1) and collected by means of a permanent magnet. This cleaning procedure was repeated at least three times to remove all free polymers originated from AIBN and unreacted monomers.

3.9. End Group Modifications of Polymer Coated Magnetic Nanoparticles

3.9.1. End Group Modification with Furan Protected Maleimide Functional Groups

Protected maleimide V-501 derivative (3) [73] (120 mg, 0.19 mmol) and polymer coated NPs (100 mg) were dissolved in 3 ml of toluene/DMF (1:1), and purged with nitrogen for 15 min. The mixture was immersed in a preheated oil bath at 70 ^{o}C for 16 h. Then, the solvent mixture was removed by rotary evaporation. NPs were dissolved in methanol, and the precipitate was removed by centrifugation. Finally, surface modified NPs were dialyzed against methanol using dialysis membrane spectra/por 7 (molecular weight cutoff 3500 Da) for 72 h.

3.9.2. End Group Modification with Azide Functional Groups

Diazido V-501 derivative (1) (96 mg, 0.18 mmol) and polymer coated NPs (100 mg) were dissolved in toluene (3 ml), and purged with nitrogen for 15 min. The mixture was immersed in a preheated oil bath at 70 ^{o}C for 16 h with vigorous stirring. After 16 h, solvent was removed by rotary evaporation, and surface modified NPs were precipitated from diethyl ether in order to remove unreacted molecules. The purified azido functionalized NPs were kept in THF for further reaction.

3.10. Activation of Maleimide Functional Groups by Retro Diels-Alder Reaction

Protected-Maleimide end group containing iron oxide NPs (75 mg) were dispersed in 20 ml of anhydrous toluene and refluxed under nitrogen protection for 16 h. After the solution cooled to room temperature, the solvent was evaporated to dryness. Magnetic NPs were dispersed in THF for further use.

3.11. Dye Conjugations with Iron Oxide Nanoparticles

3.11.1. Dye Conjugation of Maleimide Containing Polymer Coated Magnetic Nanoparticles by Thiol-Ene Reaction

End Groups maleimide modified magnetic NPs (Fe_3O_4@PEGMA-MAL3) (10 mg) and BODIPY-SH (0.1 mg) were dissolved in 200 µl of chloroform under nitrogen protection. The mixture was stirred at 37 ^oC for 16 h. After dye conjugation, unreacted dye molecules were purified adding ether to the solution and collecting NPs by means of a magnet.

3.11.2. Dye Conjugation of Azido Containing Polymer Coated Magnetic Nanoparticles by Huisgen Cycloaddition

Fe_3O_4@PEGMA@N_3-3 NPs (5 mg) were dispersed in 200 µl of THF/H_2O (3:1) mixture. Then, acetylene functionalized BODIPY (0.79 mg, 2.4 µmol) was added to the mixture, followed by addition of $CuSO_4.5H_2O$ (0.06 mg, 0.24 µmol) and sodium ascorbate (0.143 mg, 0.72 µmol). The mixture was stirred at room temperature for 16 h, and purified by precipitating ether several times.

4. RESULTS AND DISCUSSIONS

4.1. Synthesis of Iron Oxide Nanoparticles

Thermal decomposition method was used to produce highly monodisperse magnetic iron oxide NPs using the high boiling solvent 1-octadecene (Figure 4.1). Iron oleate complex, which is produced using iron (III) chloride and sodium oleate was used as precursor. Nucleation and major growth of the NPs take place by dissociation of oleate ligands between 240 – 300 ^{o}C. Decomposition of the iron oleate complex in the presence of oleic acid gives highly monodisperse iron oxide nanocrystals. During their synthesis, iron oxide NPs were coated with oleic acid stabilizing groups on in order to prevent agglomeration. Oleic acid groups possess a cis-double bond in the middle, which ensures strong stability of magnetic NPs [11]. In fact, it was found that stearic acid do not stabilize magnetic NPs due to the lack of double bond [26]. Synthesized NPs were kept in hexane for more than 6 months, and no aggregation was observed.

$$FeCl_3.6H_2O + 3\ \text{Sodium Oleate} \xrightarrow[70\ ^{o}C,\ 4\ h]{\text{Hexane, Water, Ethanol}} Fe(\text{oleate})_3 + 3\ NaCl + 6H_2O$$

$$Fe(\text{oleate})_3 + \text{Oleic Acid} \xrightarrow[320\ ^{o}C]{\text{1-octadecene}} Fe_3O_4\ \text{NPs}$$

Figure 4.1. Synthetic route of iron oxide NPs.

Oleic acid stabilized iron oxide NPs were characterized by FT-IR spectroscopy and transmission electron microscopy (TEM). The IR spectrum of SPIONs showed CH_2 asymmetric and symmetric peaks at 2915 cm^{-1} and 2846 cm^{-1}, respectively. Also, characteristic Fe-O vibration at 549 cm^{-1} proves iron oxide nanoparticle formation (Figure

4.2). Their size distribution was determined by dynamic light scattering (DLS) with diameter 7.7 nm. Furthermore, mean diameter value of the NPs was found 7.9 nm from TEM.

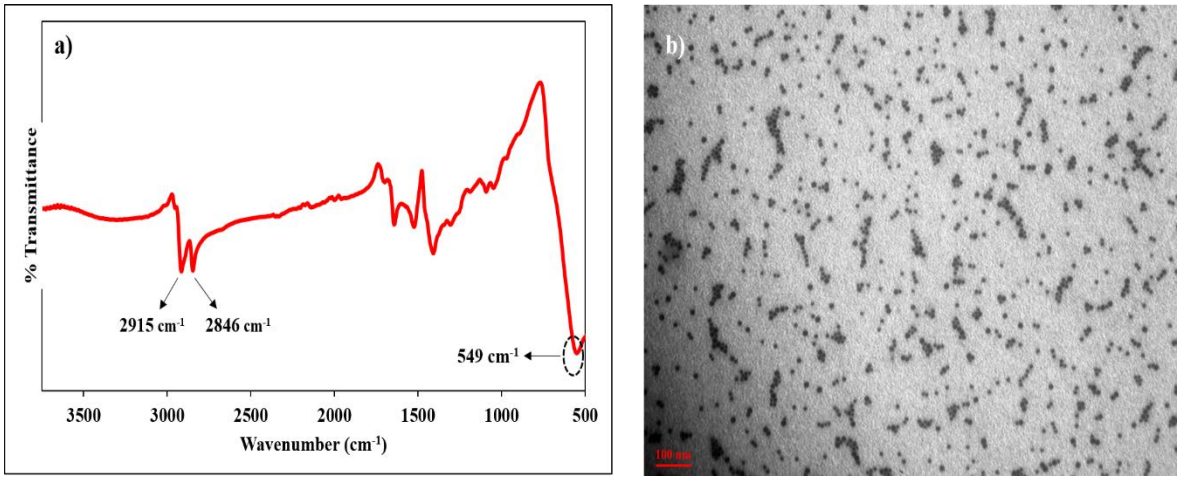

Figure 4.2. Oleic acid stabilized nanoparticles a) FT-IR spectra b) TEM image.

4.2. Modification of Chain Transfer Agent

Chain transfer agent (CTA) needed to obtain well-defined polymers was modified with catechol group (Figure 4.3) because catechol groups are known to be perfect anchoring groups for metal oxides [93]. Dopamine as bidentate enediol ligand forms a lattice structure with an octahedral geometry when it coordinates with iron oxide NPs. This structure gives rise to strong binding of dopamine to iron oxide [94]. Besides, desorption of dopamine from metal oxide is not as easy as adsorption according to Langmuir isotherms [95]. Trithiocarbonate based CTA was chosen for RAFT polymerization due to its suitability for acrylate monomers, less retardation and easy synthesis [96]. It was modified with catechol group for strong immobilization onto iron oxide so that polymers can be grown from the NP surface.

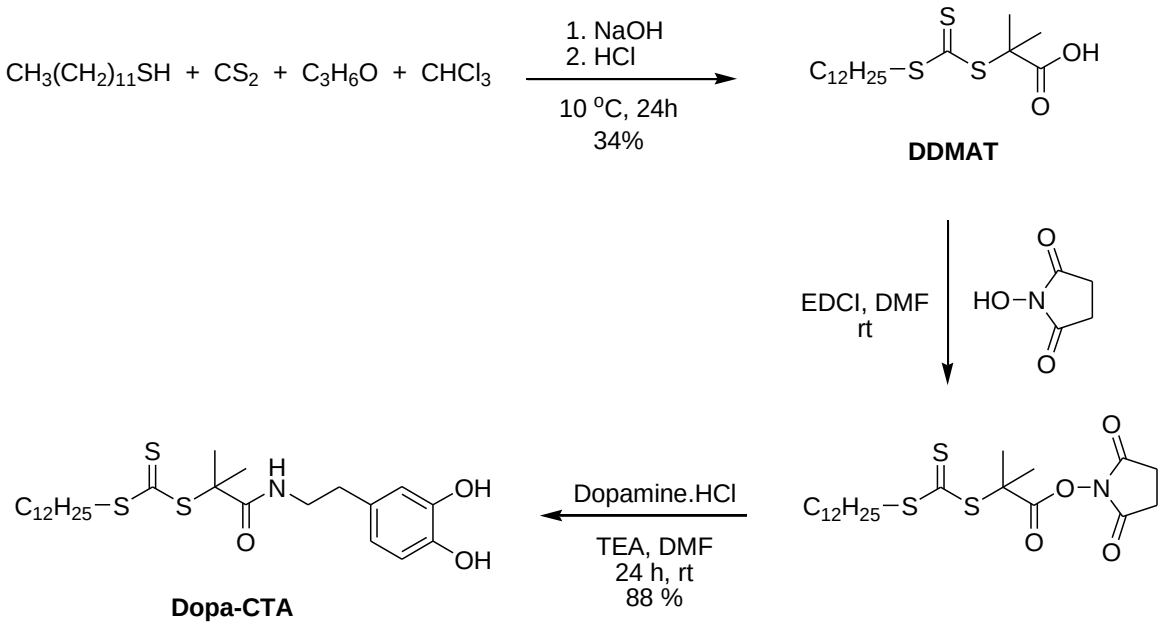

Figure 4.3. Synthesis of dopamine terminated chain transfer agent.

Trithiocarbonate based CTA was easily synthesized under strong basic environment according to literature example [89] with 34 % yield. Then, CTA was reacted with NHS in the presence of EDCI to obtain the CTA-NHS ester which was then used for dopamine conjugation. The conjugation was carried out in DMF at room temperature. Dopa-CTA was characterized by ^{1}H-NMR (Figure 4.4) and ^{13}C-NMR (Figure 4.5). According to ^{1}H NMR, the three peaks at 6.79, 6.68 and 6.56 ppm correspond to phenyl group of catechol. Two protons which are adjacent to trithiocarbonate show a triplet peak at 2.66 ppm, which proves conjugation of catechol and DDMAT successfully.

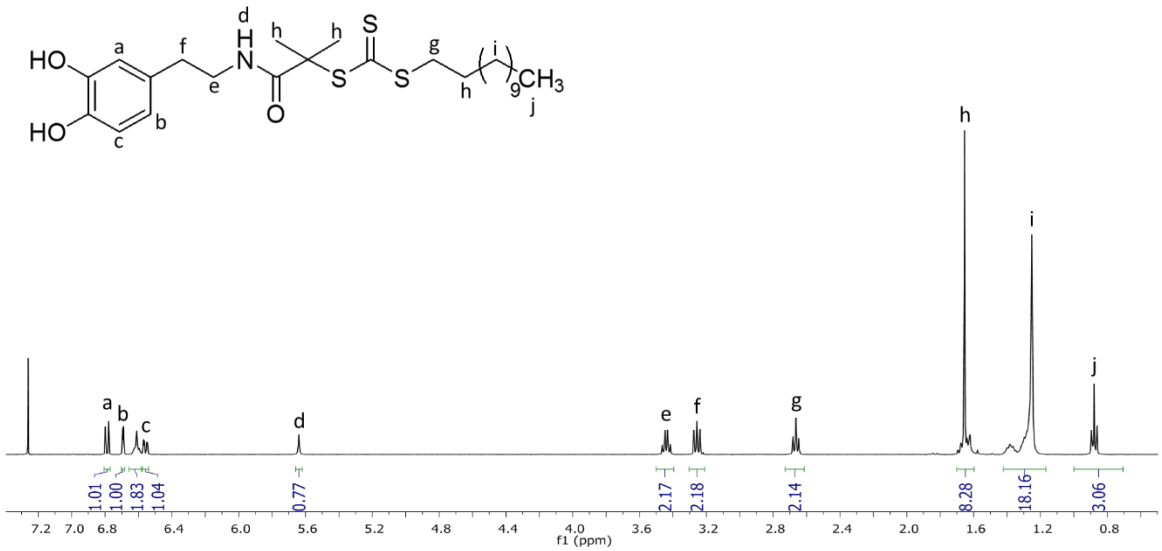

Figure 4.4. ^{1}H NMR spectrum of Dopa-CTA.

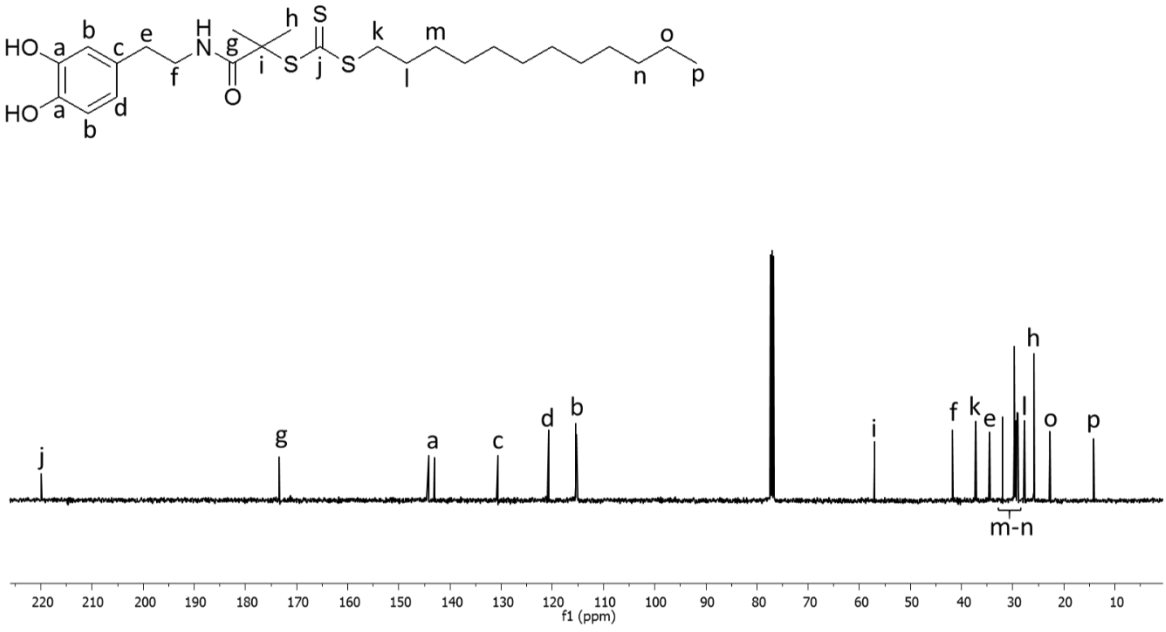

Figure 4.5. ^{13}C NMR spectrum of Dopa-CTA.

4.3. Diazido-V-501 Compound

Diazido-V-501 (1) was synthesized to have been used for end group modification of polymer coated iron oxide nanoparticles. With this approach, polymer coated nanoparticles had azido groups at the end, which could be conjugated with alkyne group by means of a click reaction. Synthesis of the compound was shown in the Figure 4.6.

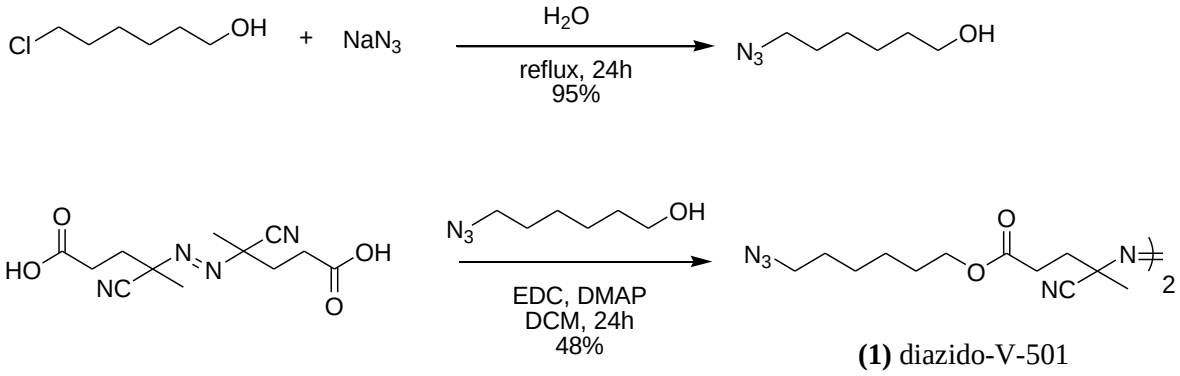

Figure 4.6. Two step synthesis of diazido-V-501 (1).

In the first step, 6-azido-1-hexanol was synthesized according to Santi's procedure [88]. The reaction was carried out under reflux for 24 h with yield of 95%. After extraction with brine, the product was used without further purification. The second step was easy esterification reaction in the presence of EDCI and DMAP. Product 1 (dizido-V-501) was purely obtained after column chromatography. ^{1}H-NMR and ^{13}C-NMR data was shown in Figure 4.7 and Figure 4.8, respectively. The ^{1}H NMR spectrum of product 1 shows the peak at 4.11 ppm coming from four ester protons. Additionally, multiplet peak at 3.27 ppm corresponds to the protons which are next to the azido groups.

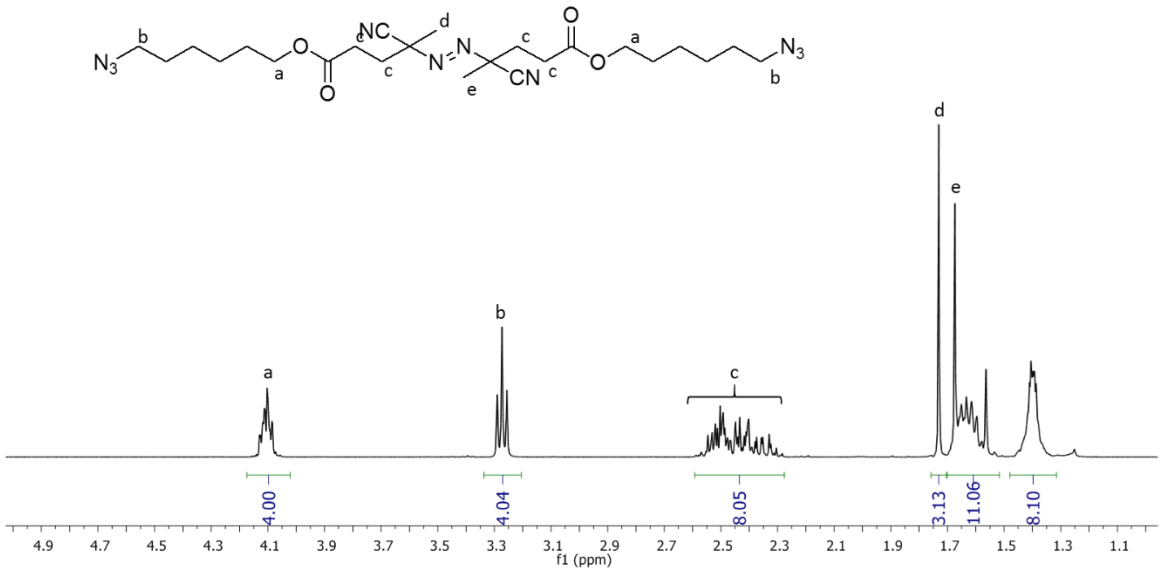

Figure 4.7. ^{1}H NMR spectrum of diazido-V-501.

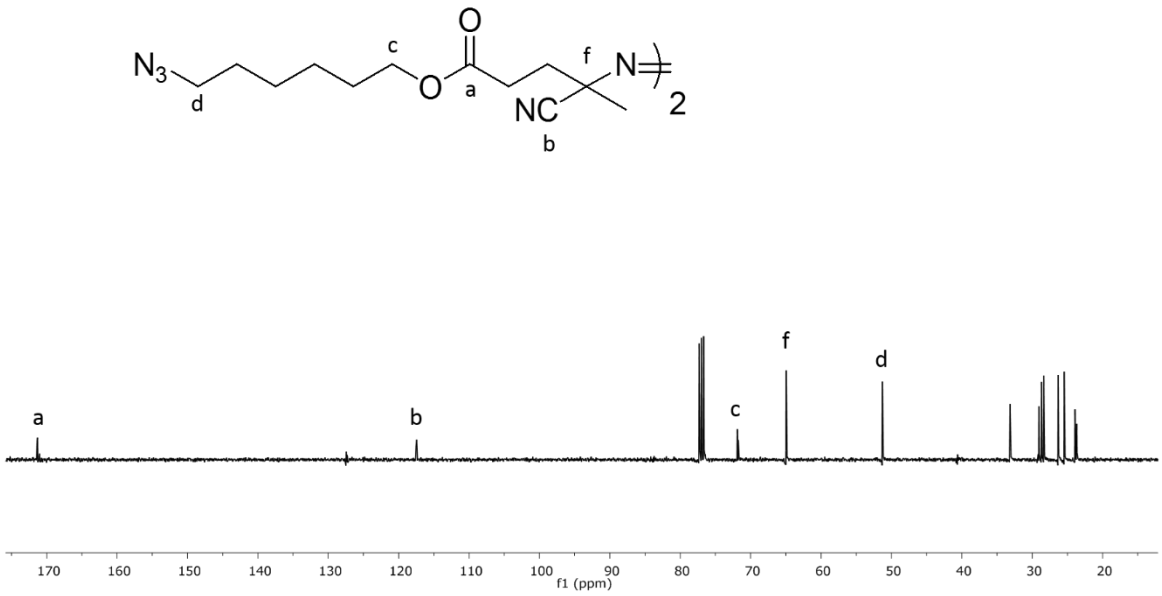

Figure 4.8. ^{13}C NMR spectrum of diazido-V-501.

4.4. Synthesis of Protected Maleimide V501 Derivative

Protected maleimide V-501 derivative (3) was synthesized according to previous literature example (Figure 4.9). The product was then used for end group modification of polymer coated iron oxide NPs via typical radical cross-coupling procedure. Trithiocarbonate end groups of the polymers were converted into protected maleimide groups. Maleimide groups can easily polymerize under radical conditions if they are not protected. Thus, maleimide groups were protected by furan groups before radical cross-coupling modification in order to prevent any side reaction.

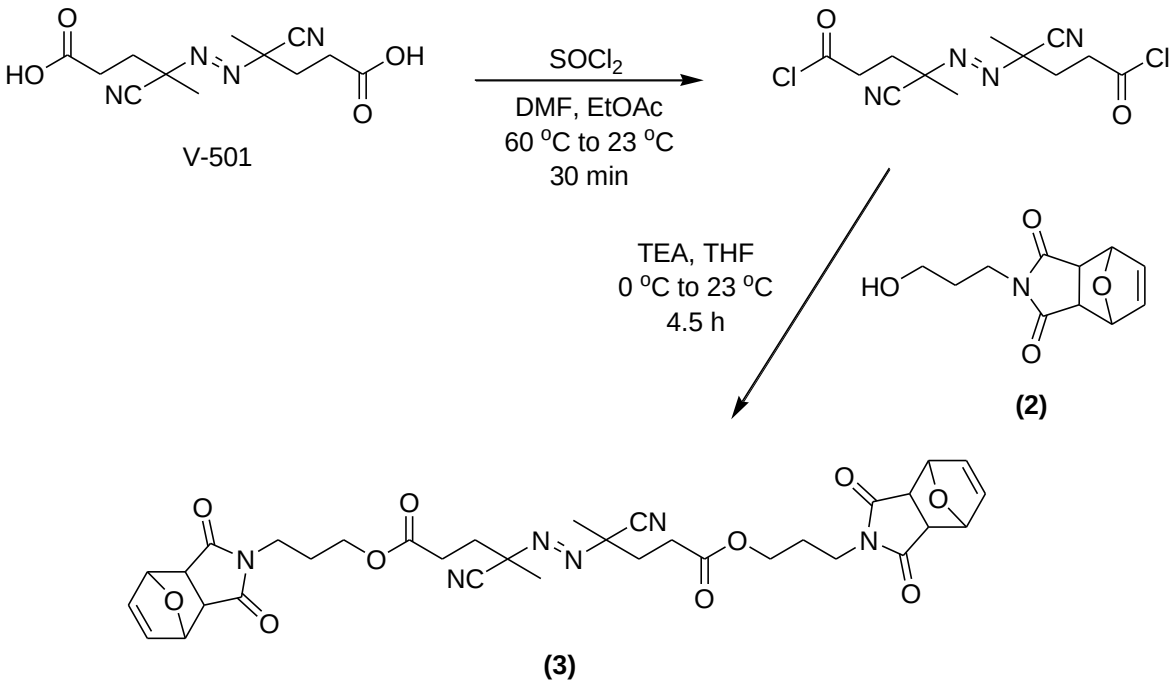

Figure 4.9. Synthesis of protected maleimide containing diazo compound (3).

V-501 was activated with thionyl chloride in the solvent mixture of DMF and EtOAc (0.05 ml / 20 ml). The product was used without further purification. Furan protected maleimide alcohol (2) was reacted with the activated V-501, and the product (3) was obtained after column chromatography as illustrated in Figure 4.9.

4.5. Chain Transfer Agent (CTA) Immobilization onto Magnetic Nanoparticles via Place Exchange Reaction

Catechol modified CTA (Dopa-CTA) was immobilized onto iron oxide NP surface by a place exchange reaction to enable the growth of the desired polymer from the surface (Figure 4.10a).

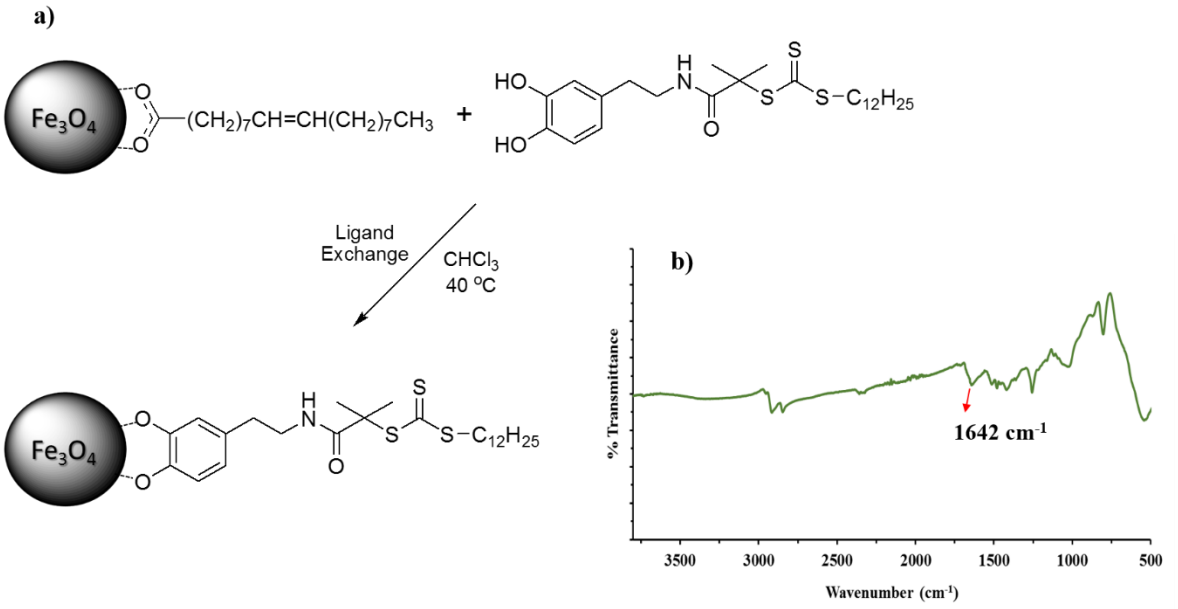

Figure 4.10. a) Dopa-CTA immobilization onto iron oxide NPs and b) FT-IR spectra of Dopa-CTA coated iron oxide NPs.

Immobilization of Dopa-CTA was carried out in $CHCl_3$ at 40 °C under nitrogen for 48 h. CTA immobilized magnetic NPs were stored in THF and never dried in order to prevent aggregation. FT-IR analysis was conducted to confirm successful attachment of Dopa-CTA (Figure 4.10b). Characteristic peak at 1642 cm^{-1} belonging to the amide carbonyl groups proved successful immobilization.

4.6. RAFT Polymerization of PEGMA with Grafting-From Manner

The procedure of surface initiated polymerization of iron oxide NPs was illustrated in Figure 4.11b. RAFT polymerization was carried out with PEGMA monomer in toluene at 70 ^{o}C under nitrogen for 24 h. PEGMA monomer was chosen for RAFT polymerization because p(PEGMA) is known to be a non-biofouling and biocompatible polymer [97]. It is also known that it decreases the iron oxide NPs uptake by macrophage cells [9].

PEGMA coated NPs were purified by precipitating from cold diethyl ether. After polymerization, polymer coated NPs could be dispersed in water since the polymer coating is water soluble. Polymer grafting was also observed by FT-IR spectroscopy (Figure 4.11a). The new peak at 1731 cm^{-1}, which belongs to carbonyl group of PEGMA units confirmed successful grow of polymers from the surface. Furthermore, PEGMA displays a strong band at 1095 cm^{-1} ascribed to the C-O-C ether stretch. Amide group carbonyl peak at 1640 cm^{-1} belonging to CTA was observed from the FT-IR spectrum.

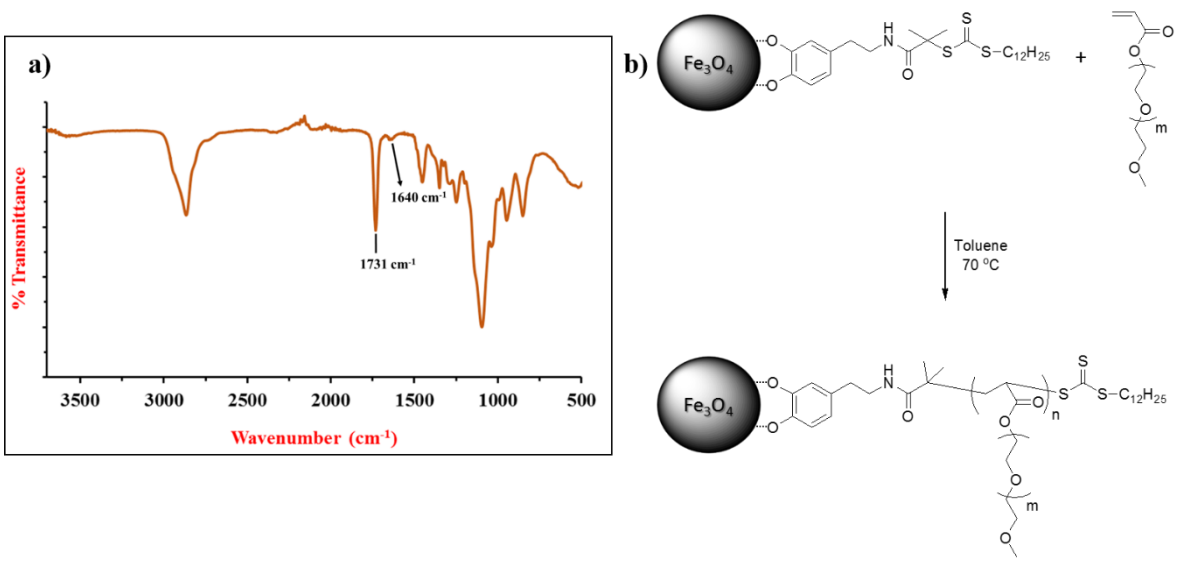

Figure 4.11. a) FT-IR spectra of polymer coated magnetic NPs b) synthesis of p(PEGMA) coated iron oxide NPs.

4.7. End Group Modifications of Polymer Coated NPs by Typical Radical Cross-Coupling Reaction

4.7.1. Modification with Protected Maleimide Azo-Initiator

Radical cross-coupling between compound (3) and polymer coated NPs was carried out at 65 ^{o}C for 16 h (Figure 4.12). The protected maleimide groups were attached at the ω chain end. After cross-coupling reaction, protected maleimide containing NPs were dissolved in methanol. The insoluble residual was removed by centrifugation, and the solution was then dialyzed against methanol for 72 h to get purified protected maleimide functionalized iron oxide NPs (Fe_3O_4@PEGMA-pMAL).

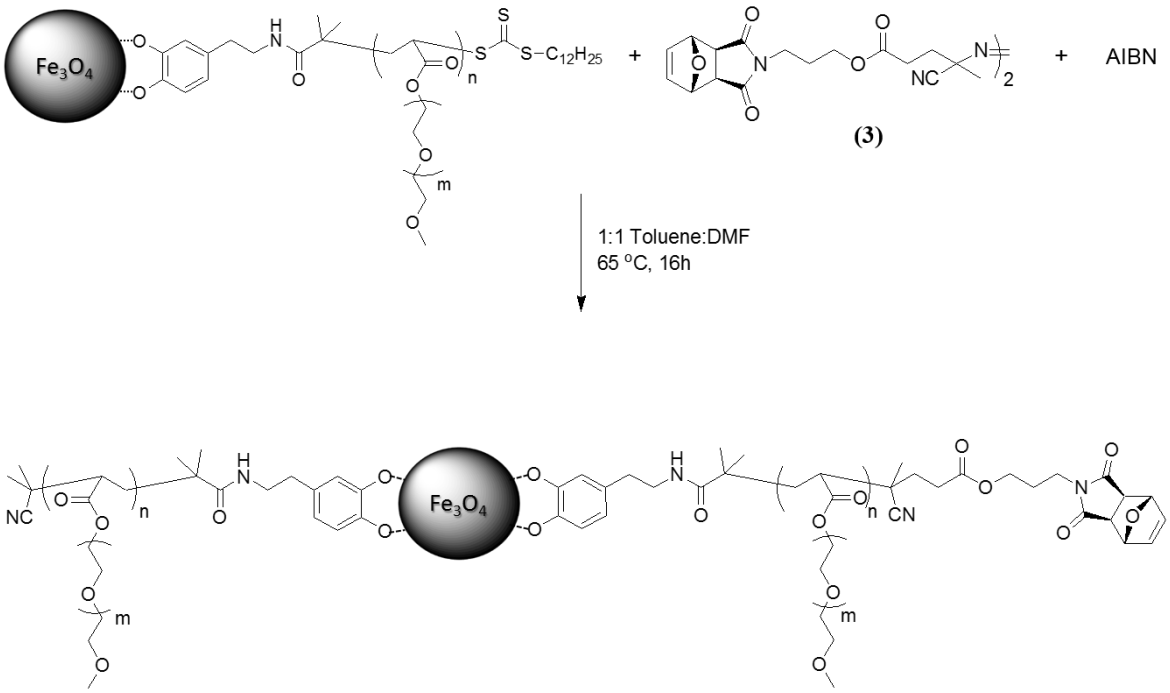

Figure 4.12. End group modification of magnetic NPs by protected maleimide group and AIBN.

Furan protected maleimide groups were investigated with different ratios with respect to AIBN as illustrated in Table 4.1. Using cross coupling methodology, we were able

to bear maleimide groups onto iron oxide NP surface with different ratios. After successful modification of protected maleimide groups, these groups were activated by retro Diels-Alder reaction for further functionalization.

Table 4.1. End groups maleimide modified NPs according to AIBN/Maleimide ratio before and after retro Diels-Alder reaction.

Before retro Diels-Alder	Maleimide (%)	AIBN (%)	After retro Diels-Alder	Maleimide (%)	AIBN (%)
Fe_3O_4@PEGMA-pMAL1	25	75	Fe_3O_4@PEGMA-MAL1	25	75
Fe_3O_4@PEGMA-pMAL2	50	50	Fe_3O_4@PEGMA-MAL2	50	50
Fe_3O_4@PEGMA-pMAL3	100	0	Fe_3O_4@PEGMA-MAL3	100	0

The end group ratios were probed by FT-IR measurements and found that transmittance of new carbonyl peak belonging to maleimide groups increased when the compound (3) ratio was increased. The protected maleimide groups were characterized by FT-IR spectroscopy (Figure 4.13). Characteristic peak of protected maleimide carbonyl groups at 1701 cm^{-1} appeared after cross-coupling reaction of compound (3), and the peak sharpened with increase of protected maleimide end groups. This result indicated that it was possible to install functional groups onto iron oxide NP surface with varying density. We used protected maleimide/AIBN groups modified NPs for dye conjugation after deprotection of furan, and we was able to disperse polymer coated NPs in water even after attachment of the hydrophobic dye BODIPY.

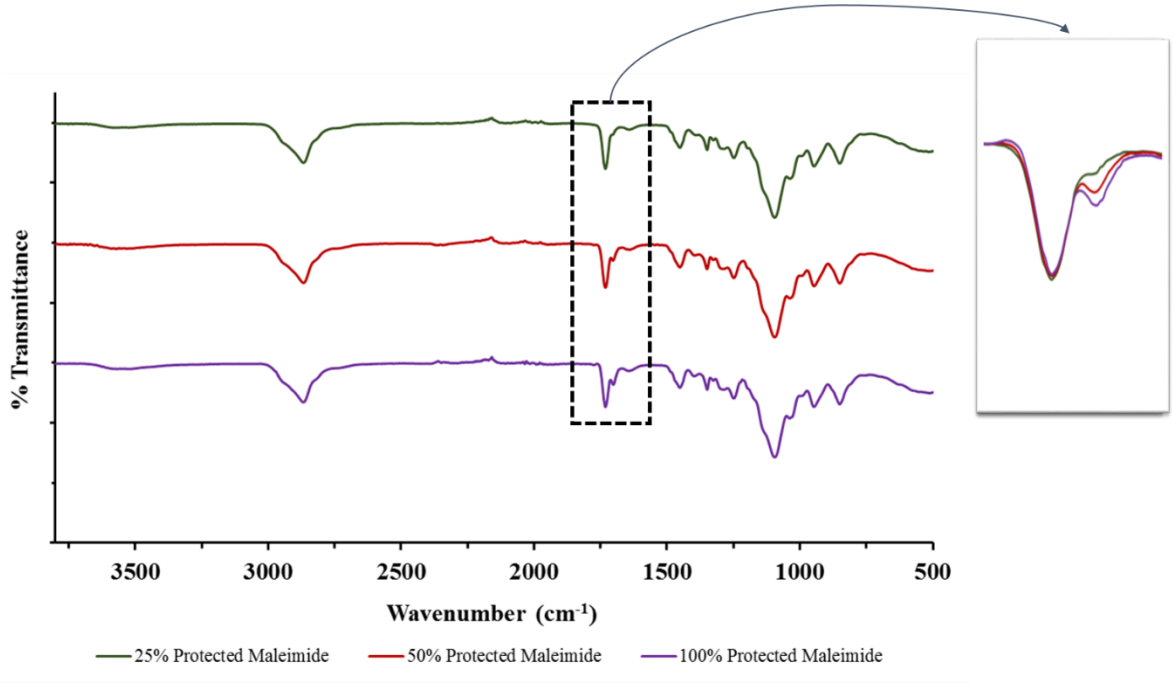

Figure 4.13. FT-IR spectra of furan protected maleimide terminated iron oxide NPs.

4.7.2 Activation of Maleimide Groups by Retro Diels-Alder Reaction

Maleimide groups were protected with furan before cross-coupling reaction in order to prevent radical polymerization of maleimide. End groups protected maleimide modified NPs were activated by retro Diels-Alder reaction. The reaction was carried out in toluene at 110 ^{o}C for 16 h (Figure 4.14).

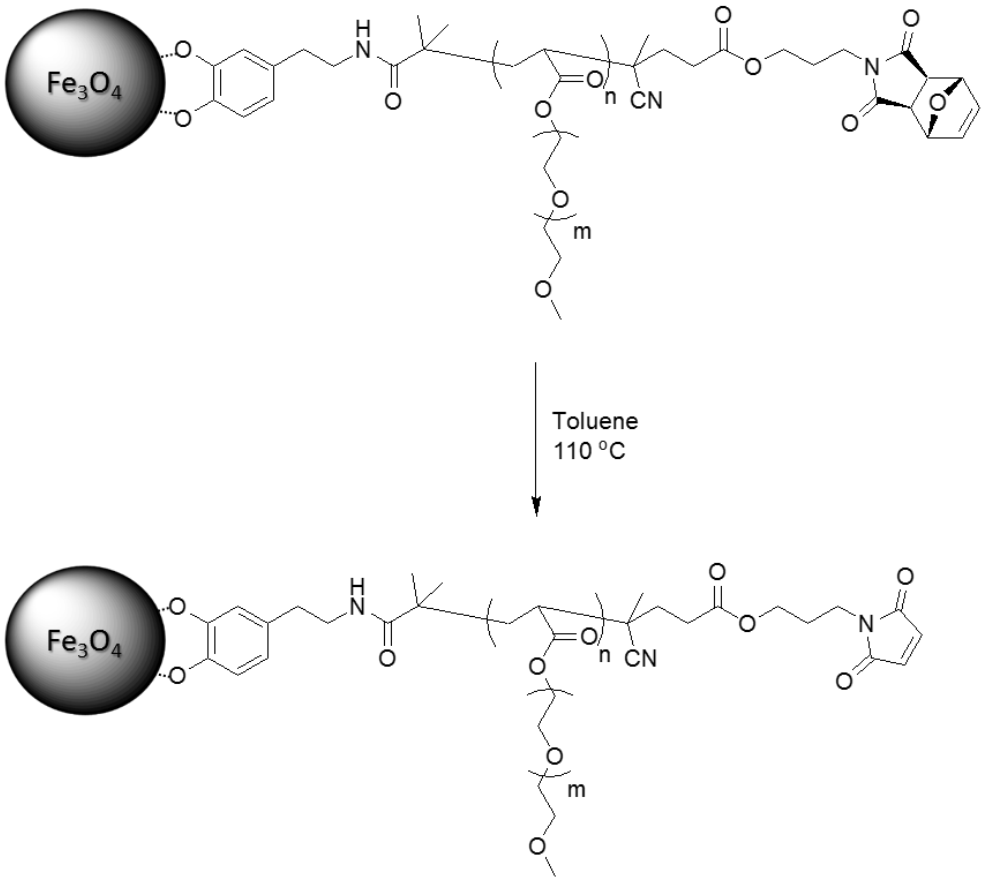

Figure 4.14. End group activation of magnetic NPs by retro Diels-Alder reaction.

Maleimide groups containing reactive polymers have been used for conjugation to proteins [98] and other thiol-containing biomolecules. On the basis of this fact, we modified iron oxide NPs' end groups with maleimide groups, which can easily react with thiol without any other reagent in mild conditions to achieve functionalization.

Figure 4.15 shows FT-IR spectra of maleimide end group containing NPs (Fe_3O_4@MAL) with different ratios after retro Diels-Alder reaction (Figure 4.14).

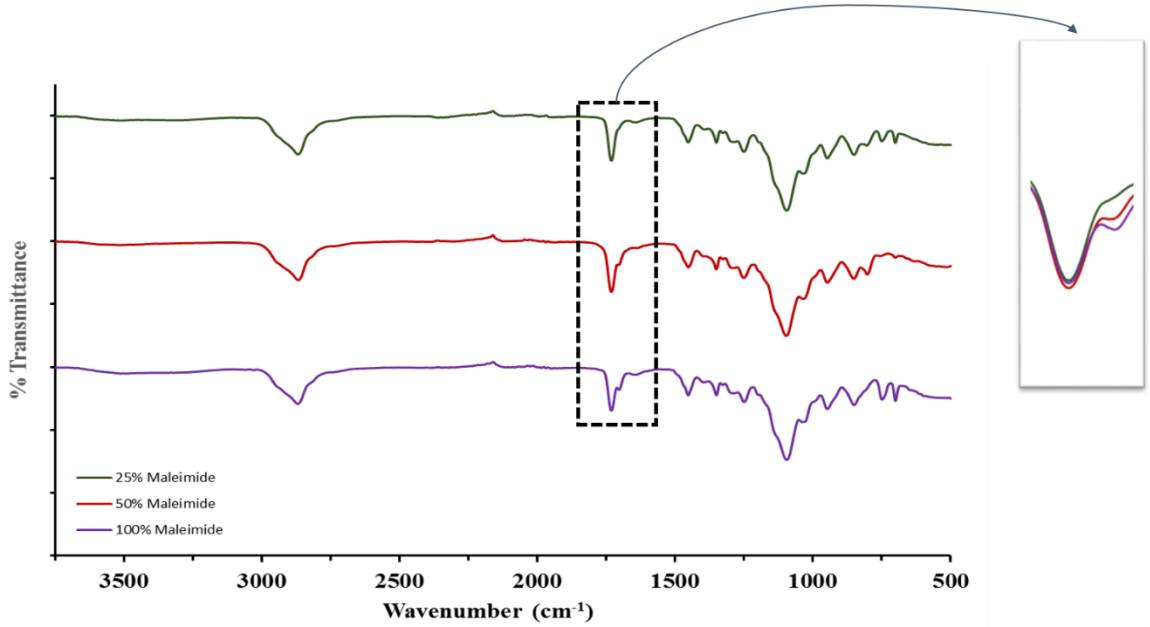

Figure 4.15. FT-IR spectra of maleimide terminated iron oxide NPs.

4.7.3. Modification with Azido Bearing Azo-Initiator

Polymer coated magnetic NPs which have trithiocarbonate groups at the end of polymer chain was reacted with an excess of compound (1) to generate azido groups at the end using cross-coupling reaction (Figure 4.16). The reaction was performed under nitrogen protection at 65 ^{o}C for 16 h with 20-fold excess diazido-V-501 compound. End groups functionalized NPs were purified via precipitating from cold diethyl ether and collected by centrifugation. In the FT-IR spectrum, a band owing to the stretching of the azide group was noticed at 2096 cm^{-1}, which confirmed that the cross-coupling reaction had been successful (Figure 4.17).

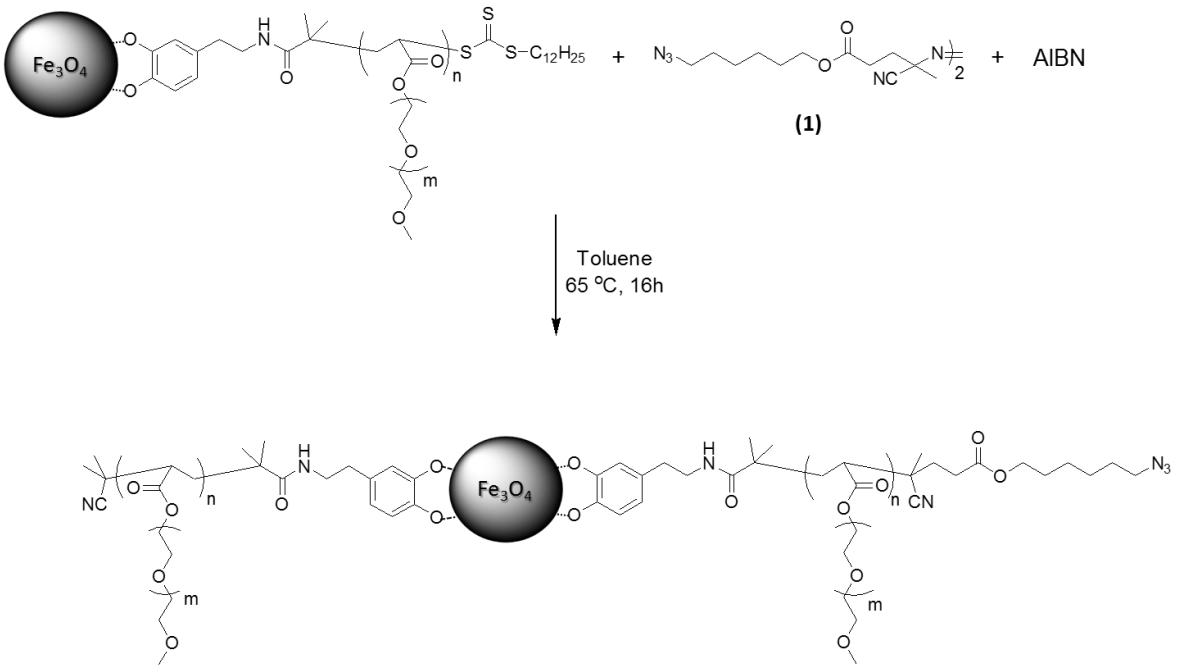

Figure 4.16. End group modification of magnetic NPs by azido groups and AIBN.

We attempted azido group modification in the presence of AIBN in order to show efficiency of controlling end groups density. Table 4.2 displays the ratio of compound (1) and AIBN used for modification of the end groups.

Table 4.2. End groups azido modified NPs according to AIBN/Azido ratio.

No	Modified NPs	Diazido-V-501 (%)	AIBN (%)
1	Fe_3O_4@PEGMA@N_3-1	25	75
2	Fe_3O_4@PEGMA@N_3-2	50	50
3	Fe_3O_4@PEGMA@N_3-3	100	0

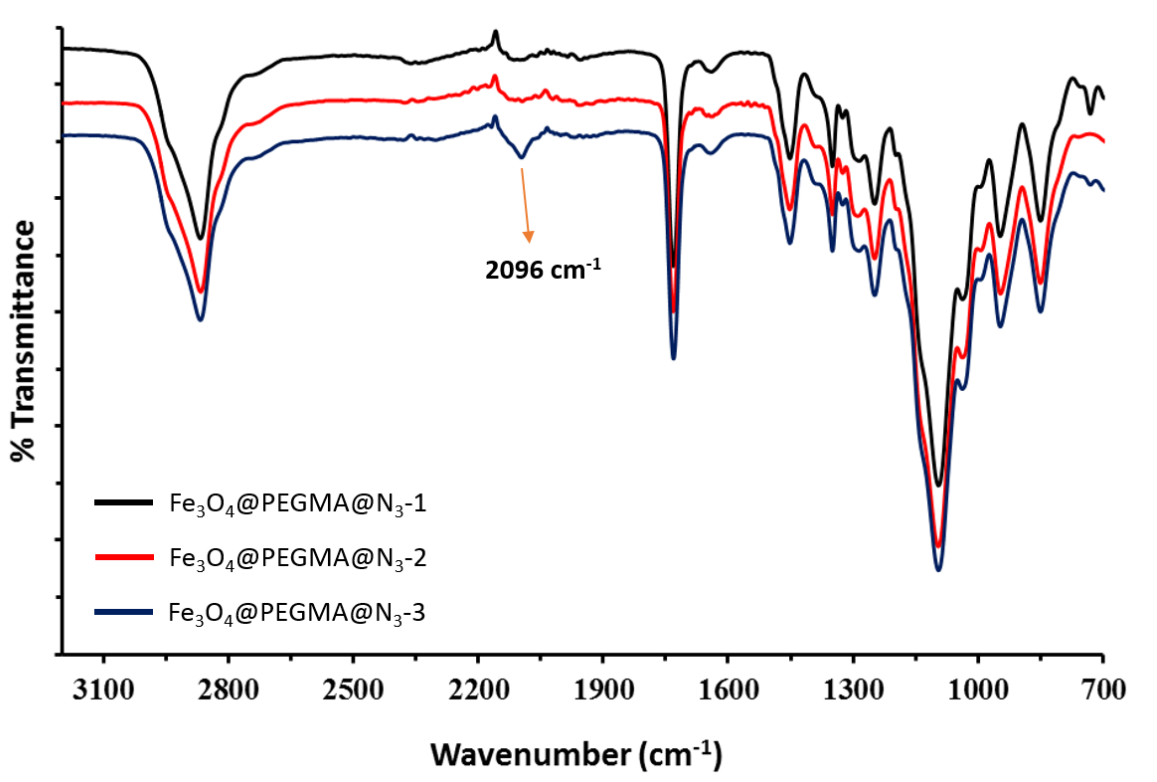

Figure 4.17. FT-IR spectra of azido group terminated magnetic NPs

4.8. Functionalization of Polymer Coated Nanoparticles

4.8.1. Nucleophilic Thiol-Ene Reaction

Functionalization of polymer coated NPs using Michael addition was investigated. Maleimide end group containing polymer modified iron oxide NPs (Fe_3O_4@MAL3) were conjugated with BODIPY-SH in chloroform at 37 ^oC for 16 h (Figure 4.18). This functionalization could be achieved under mild and reagent free conditions.

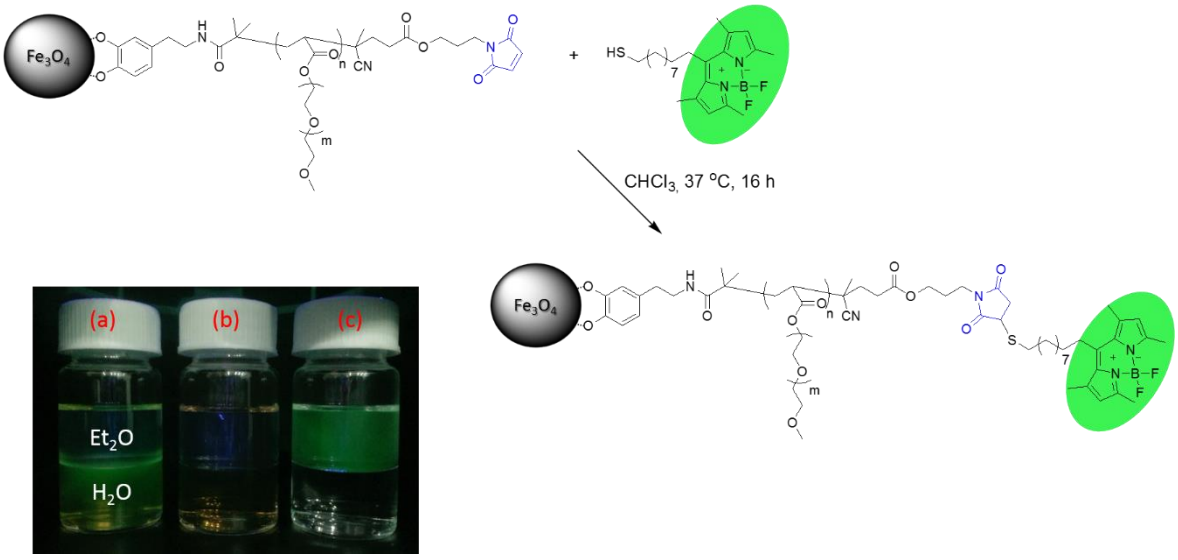

Figure 4.18. Dye conjugation onto maleimide groups terminated iron oxide NPs by thiol-ene chemistry a) dye attached NPs b) control c) free dye.

Dye conjugated NPs were purified by precipitating from ether whereby the free dye was dissolved in ether and easily removed. After dye conjugation, NPs were dispersed in water and gave fluorescent under UV illumination. As a control experiment, end groups protected maleimide containing NPs was used. Dye attachment experiment was conducted under same conditions; however, thiol bearing dye (BODIPY-SH) did not react with protected maleimide groups. This was inferred from lack of any fluorescence under UV illumination.

4.8.2. Huisgen Cyloaddition Reaction

Attachment of hydrophobic BODIPY-alkyne dye onto iron oxide NP surface was investigated. Azide functionalized magnetic NPs (Fe_3O_4@PEGMA@N_3-3) were dissolved in a solvent mixture of THF/H_2O and dye was attached onto iron oxide surface by Huisgen type click chemistry in the presence of copper and reducing agent sodium ascorbate (Figure 4.18). Dye attachment was readily observed after purification of all free dye. As illustrated

in Figure 4.18c, dye attached NPs were dispersed in water and gave fluorescent under UV illumination, and there was no dye fluorescence in ether phase.

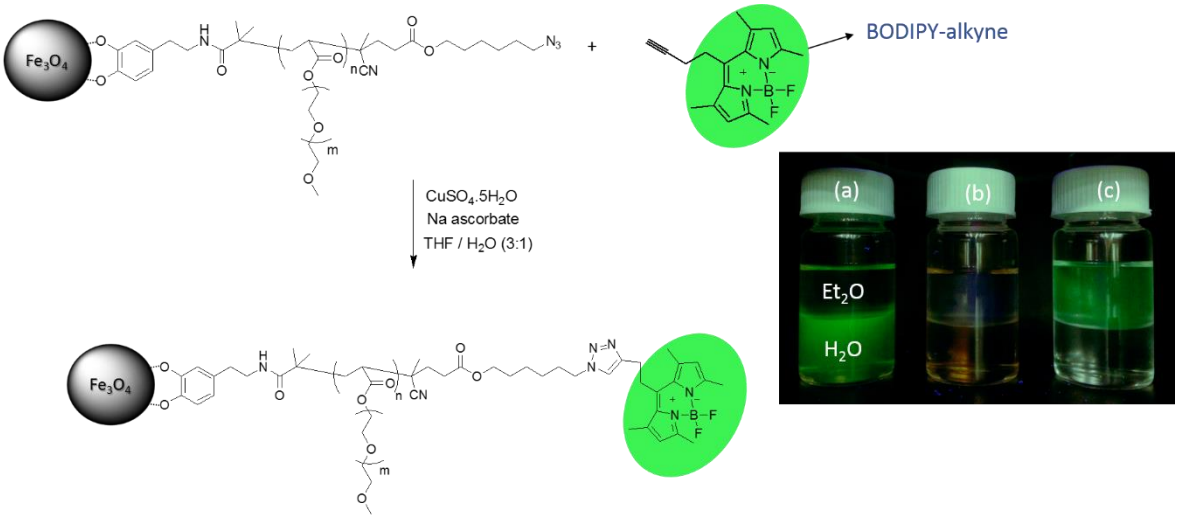

Figure 4.19. Dye conjugation onto azido groups terminated iron oxide NPs by Huisgen click chemistry a) dye attached NPs b) control c) free dye.

As a control experiment, the NPs were mixed with BODIPY-alkyne in the absence of copper catalyst, and there was no attachment of dye onto iron oxide NPs, which proved the attachment was not due to physical interactions (Figure 4.18b).

4.10. Thermal Gravimetric Analysis of Iron Oxide NPs

TGA curves of parent NPs (Fe_3O_4@OA), CTA immobilized NPs (Fe_3O_4@CTA) and polymer coated NPs (Fe_3O_4@PEGMA) were illustrated in Figure 4.21. In order to determine organic contents of NPs, TGA is a useful method since organic contents completely degrade between 300 - 400 ^oC. Oleic acid coated NPs gave 24 % weight loss. After ligand exchange with Dopa-CTA, it was observed that two stage decomposition profile. This was attributed to oleic acid residuals on iron oxide NP surface. After 6 h polymerization with PEGMA

monomer, the weight loss of NPs was significantly higher, indicating that polymer was successfully grown from the surface (90 % weight loss).

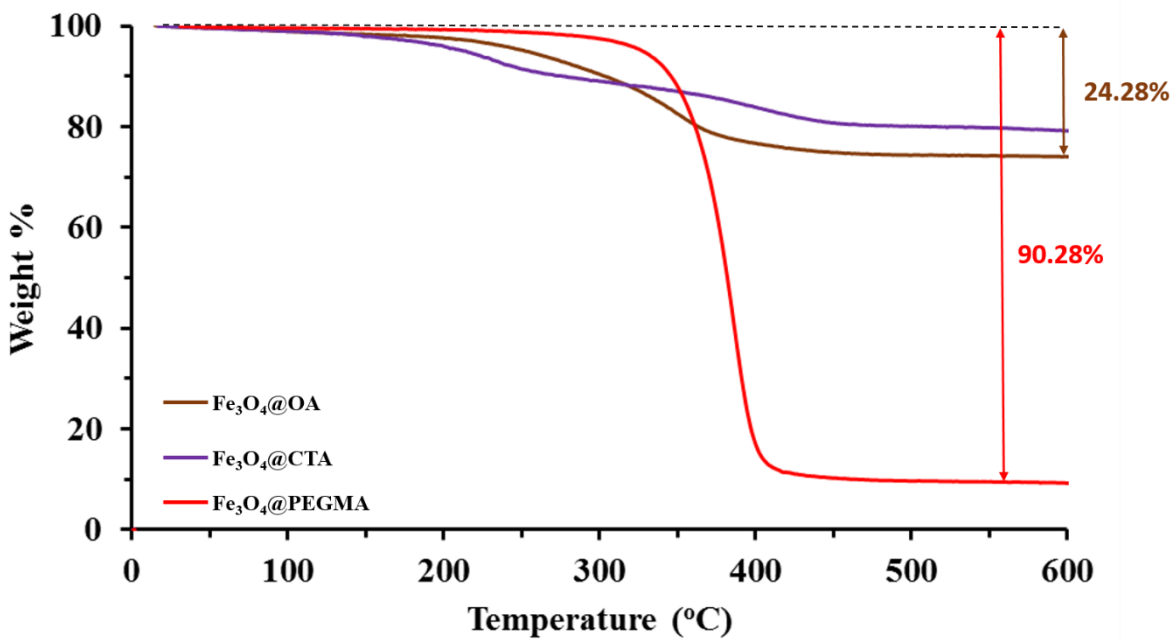

Figure 4.20. TGA curves of Fe_3O_4@OA, Fe_3O_4@CTA and Fe_3O_4@PEGMA

4.11. Dynamic Light Scattering Measurements of Iron Oxide NPs

DLS was used to monitor hydrodynamic size of parent magnetic NPs, after RAFT polymerization, and also after CTA immobilization. Oleic acid coated NPs were dispersed in hexane; whereas polymer coated and CTA immobilized NPs were dispersed in DMF before measurements were carried out. Figure 4.22 shows the hydrodynamic sizes of magnetic NPs.

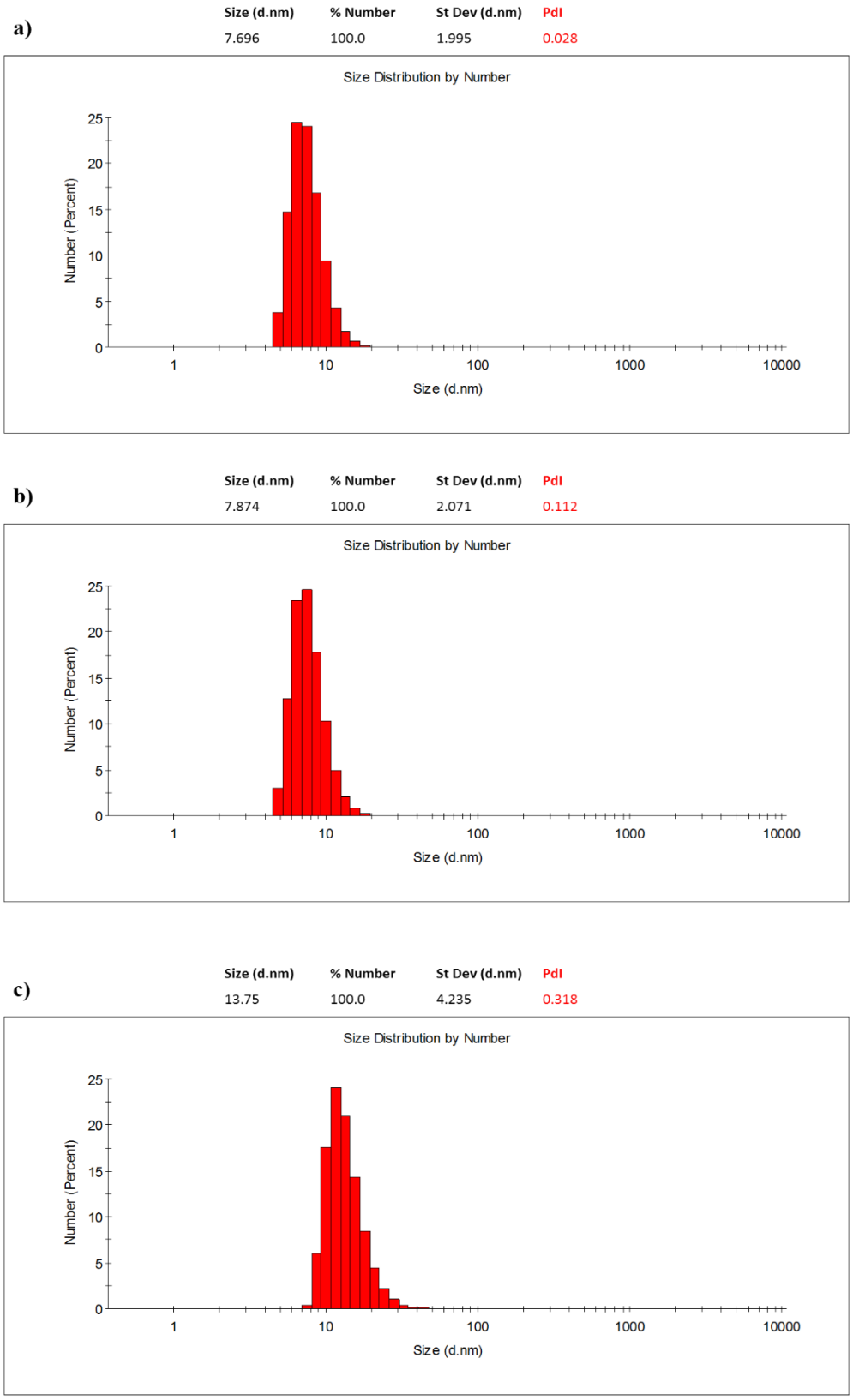

Figure 4.21. DLS analysis of iron oxide NPs a) Fe_3O_4@OA b) Fe_3O_4@CTA and c) Fe_3O_4@PEGMA

Fe_3O_4@OA size was 7.7 nm with very low PDI, which showed that they had the same size distribution profile by number (Figure 4.22a). After place exchange reaction with catechol terminated CTA, we measured the diameter of NPs 7.9 nm (Figure 4.22b). This result is expected because chain lengths of oleic acid and Dopa-CTA are approximately the same. Polymer grow from NPs' surface was proved by DLS measurements with diameter of 13.7 nm (Figure 4.22c). Hydrodynamic size of NPs increased approximately 5 nm after polymerization, showing that it is possible to grow water dispersible NPs by RAFT polymerization.

Size distribution of iron oxide NPs after end group modification process was also examined in order to show whether NPs form aggregates during the radical based chain end modification. For DLS analysis, 100% functional end group containing NPs, Fe_3O_4@PEGMA-pMAL3 and Fe_3O_4@PEGMA@N_3-3, were chosen. After cross-coupling modification, the hydrodynamic sizes of Fe_3O_4@PEGMA-pMAL3 and Fe_3O_4@PEGMA@N_3-3 are 12.44 nm and 13.69 nm, respectively (Figure 4.23).

Protected maleimide groups containing NPs were activated by a retro Diels-Alder reaction. Dynamic light scattering measurement was examined for Fe_3O_4@PEGMA-MAL3 to show if any crosslinking occurred between maleimide groups during activation reaction. It was found that there was no aggregation, and the diameter of maleimide ended NPs was 12.5 nm (Figure 4.23b).

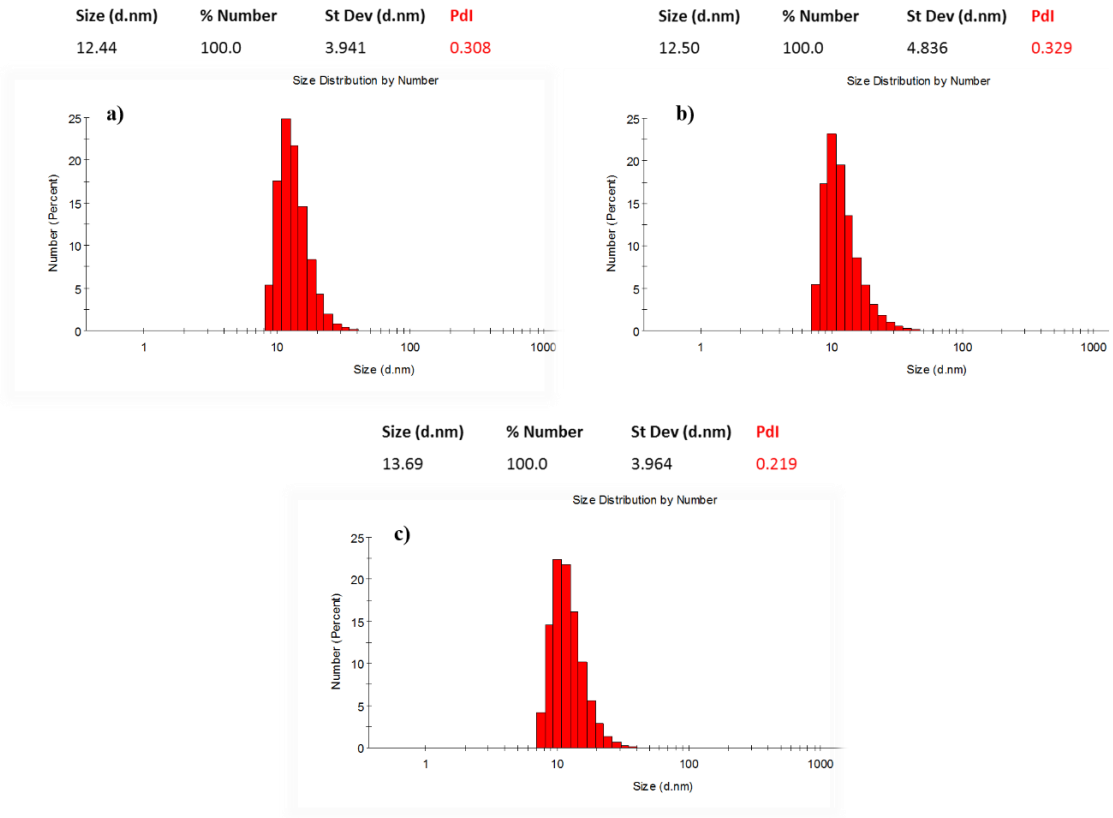

Figure 4.22. DLS analysis of NPs a) Fe_3O_4@PEGMA-pMAL3 b) Fe_3O_4@PEGMA-MAL3 c) Fe_3O_4@PEGMA@N_3-3.

4.12. Transmission Electron Microscopy (TEM)

TEM images of magnetic NPs were taken from LVEM5 microscope by placing a drop on a carbon coated copper grid. As shown in Figure 4.24a, oleic acid coated NPs were well dispersed with a particle size of 7.9 nm. After place exchange reaction, CTA was immobilized onto iron oxide NP surface. TEM image of CTA immobilized NPs is shown in Figure 4.24b. They are completely uniform with diameter of 7.8 nm. Figure 4.24c shows polymer coated NP's image after 24 h RAFT polymerization. Organic layer cannot be visible owing to the lack of contrast between background and the organic shell. Nevertheless, these NPs were examined with DLS and IR, and we found that polymer growth was successful. TEM image show NPs do not form aggregation during polymerization. Finally, end group modified NPs were studied by TEM (Figure 4.24d and 4.24e). Even after radical cross coupling modification, NPs remained highly uniform, which is important for most of the applications of magnetic NPs.

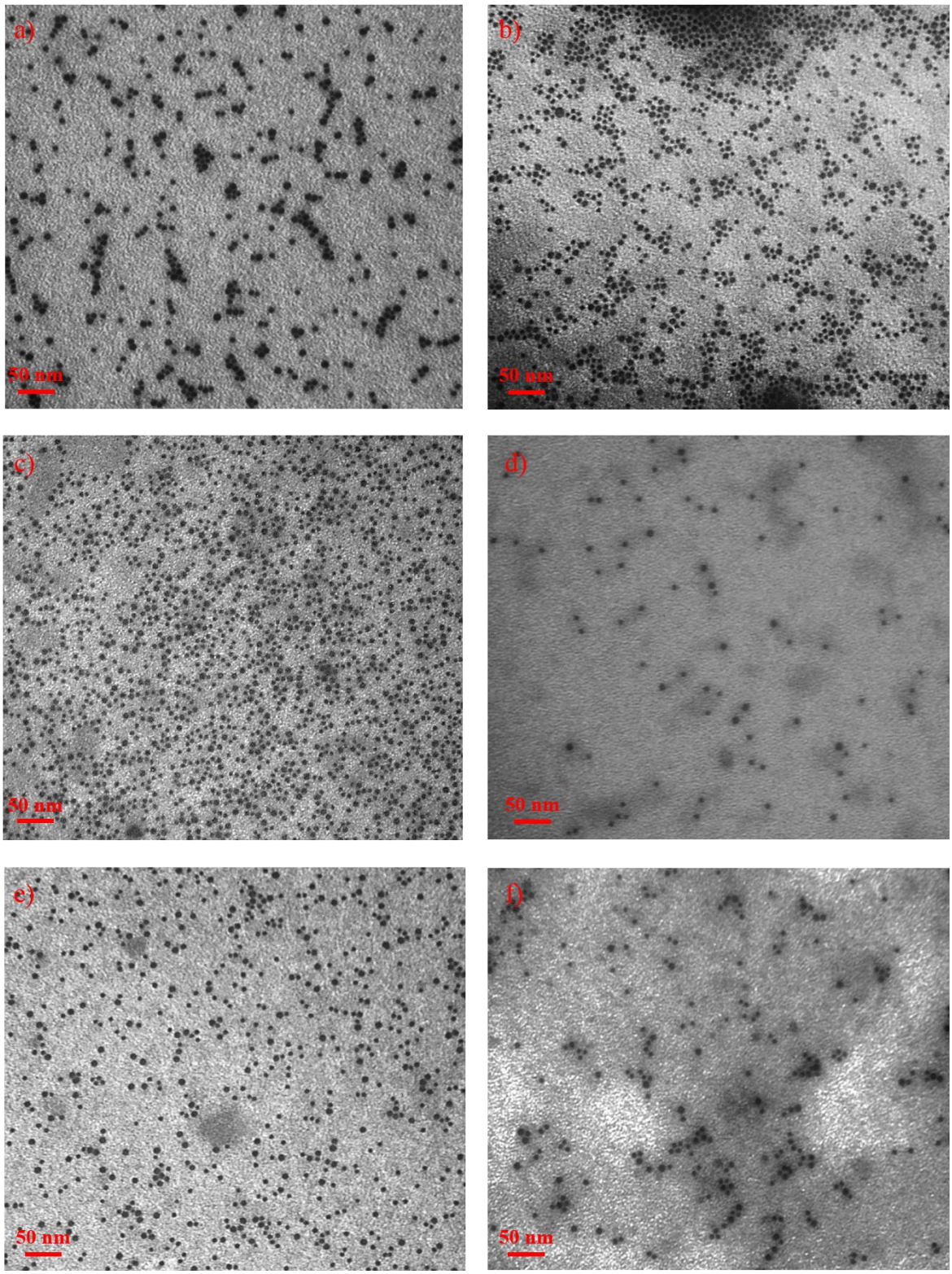

Figure 4.23. TEM images of magnetic NPs a) Fe_3O_4@OA, b) Fe_3O_4@CTA, c) Fe_3O_4@PEGMA, d) Fe_3O_4@PEGMA-pMAL3, e) Fe_3O_4@PEGMA@N_3-3 and f) Fe_3O_4@PEGMA-MAL3.

5. CONCLUSION

Magnetic NPs grafted with PEG-based polymer containing reactive end groups at chain-ends were synthesized with a graft-from approach. Well-defined magnetic NPs with 8 nm diameter were synthesized using thermal decomposition procedure. Magnetic NPs were efficiently coated with p(PEGMEA) polymers using RAFT polymerization in the presence of trithiocarbonate based chain transfer agent which was immobilized onto iron oxide NP surface. Ω-end groups of the polymers attached to the nanoparticles are modifiable, and different modifications can be performed according to desired application. In this thesis, radical cross-coupling reaction was utilized to modify end groups of the polymer. In order to install maleimide and azido functional groups onto magnetic NP surface, modified azo-initiators were synthesized. Radical exchange reaction by heating the polymer coated NPs in the presence of reactive functional group bearing azo compounds led to desired chain end modifications. A furan protected maleimide group and an azide group were incorporated at chain ends using this approach. Magnetic NPs containing a thiol-reactive maleimide group at polymer chain ends was obtained by heating the furan-protected maleimide containing polymer coated NPs. After end group modification, the maleimide containing NPs were functionalized with thiol containing fluorescent BODIPY dye, and the azido group containing NPs were functionalized with alkyne containing fluorescent BODIPY dye.

REFERENCES

1. Yallapu, M. M., S. F. Othman, E. T. Curtis, B. K. Gupta, M. Jaggi, and S. C. Chauhan, "Multi-Functional Magnetic Nanoparticles for Magnetic Resonance Imaging and Cancer Therapy", *Biomaterials*, Vol. 32, pp. 1890–1905, 2011.

2. Liong, M., J. Lu, M. Kovochich, T. Xia, S. G. Ruehm, A. E. Nel, F. Tamanoi, and J. I. Zink, "Multifunctional Inorganic Nanoparticles for Imaging, Targeting, and Drug Delivery", *ACS Nano*, Vol. 2, pp. 889–896, 2008.

3. Zhang, L., Y. Wang, Y. Tang, Z. Jiao, C. Xie, H. Zhang, P. Gu, X. Wei, G. Y. Yang, H. Gu, and C. Zhang, "High MRI Performance Fluorescent Mesoporous Silica-Coated Magnetic Nanoparticles for Tracking Neural Progenitor Cells in an Ischemic Mouse Model", *Nanoscale*, Vol. 5, pp. 4506–4516, 2013.

4. Lin, P. C., C. C. Yu, H. T. Wu, Y. W. Lu, C. L. Han, A. K. Su, Y. J. Chen, and C. C. Lin, "A Chemically Functionalized Magnetic Nanoplatform for Rapid and Specific Biomolecular Recognition and Separation", *Biomacromolecules*, Vol. 14, pp. 160–168, 2013.

5. Xu, C. and S. Sun, "Monodisperse Magnetic Nanoparticles for Biomedical Applications", *Polymer International*, Vol. 56, pp. 821–826, 2007.

6. Boyer, C., V. Bulmus, P. Priyanto, W. Y. Teoh, R. Amal, and T. P. Davis, "The Stabilization and Bio-Functionalization of Iron Oxide Nanoparticles Using Heterotelechelic Polymers", *Journal of Materials Chemistry*, Vol. 19, p. 111, 2009.

7. Laurent, S., D. Forge, M. Port, A. Roch, C. Robic, L. Vander Elst, and R. N. Muller, "Magnetic Iron Oxide Nanoparticles: Synthesis, Stabilization, Vectorization, Physicochemical Characterizations, and Biological Applications", *Chemical Reviews*, Vol. 108, pp. 2064–2110, 2008.

8. Lu, A. H., E. L. Salabas, and F. Schüth, "Magnetic Nanoparticles: Synthesis, Protection, Functionalization, and Application", *Angewandte Chemie International Edition*, Vol. 46, pp. 1222–1244, 2007.

9. Kang, S. M., I. S. Choi, K. Lee, and Y. Kim, “Bioconjugation of Poly(Poly(Ethylene Glycol) Methacrylate)-Coated Iron Oxide Magnetic Nanoparticles for Magnetic Capture of Target Proteins”, *Macromolecular Research.*, Vol. 17, pp. 259–264, 2009.

10. Lee, H., E. Lee, D. K. Kim, N. K. Jang, Y. Y. Jeong, and S. Jon, “Antibiofouling Polymer-Coated Superparamagnetic Iron Oxide Nanoparticles as Potential Magnetic Resonance Contrast Agents for in Vivo Cancer Imaging”, *Journal of the American Chemical Society*, Vol. 128, pp. 7383–7389, 2006.

11. Wu, W., Q. He, and C. Jiang, “Magnetic Iron Oxide Nanoparticles: Synthesis and Surface Functionalization Strategies”, *Nanoscale Research Letters*, Vol. 3, pp. 397–415, 2008.

12. Briley-Saebo, K., A. Bjørnerud, D. Grant, H. Ahlstrom, T. Berg, and G. M. Kindberg, “Hepatic Cellular Distribution and Degradation of Iron Oxide Nanoparticles Following Single Intravenous Injection in Rats: Implications for Magnetic Resonance Imaging”, *Cell Tissue Research*, Vol. 316, pp. 315–23, 2004.

13. Kim, B. H., N. Lee, H. Kim, K. An, Y. Il Park, Y. Choi, K. Shin, Y. Lee, S. G. Kwon, H. Bin Na, J.-G. Park, T.-Y. Ahn, Y.-W. Kim, W. K. Moon, S. H. Choi, and T. Hyeon, “Large-Scale Synthesis of Uniform and Extremely Small-Sized Iron Oxide Nanoparticles for High-Resolution T1 Magnetic Resonance Imaging Contrast Agents”, *Journal of the American Chemical Society*, Vol. 133, pp. 12624–12631, 2011.

14. Song, M., Y. Zhang, S. Hu, L. Song, J. Dong, Z. Chen, and N. Gu, “Influence of Morphology and Surface Exchange Reaction on Magnetic Properties of Monodisperse Magnetite Nanoparticles”, *Colloids and Surfaces A: Physicochemical Engineering Aspects*, Vol. 408, pp. 114–121, 2012.

15. Santra, S., R. Tapec, N. Theodoropoulou, J. Dobson, A. Hebard, and W. Tan, “Synthesis and Characterization of Silica-Coated Iron Oxide Nanoparticles in Microemulsion: The Effect of Nonionic Surfactants”, *Langmuir*, Vol. 17, pp. 2900–2906, 2001.

16. Lutz, J.-F., S. Stiller, A. Hoth, L. Kaufner, U. Pison, and R. Cartier, “One-Pot Synthesis of Pegylated Ultrasmall Iron-Oxide Nanoparticles and Their in Vivo Evaluation as Magnetic Resonance Imaging Contrast Agents”, *Biomacromolecules*, Vol. 7, pp. 3132–3138, 2006.

17. Grene, J. M., P. Bernhardt, C. Leuvrey, G. Rogez, L. Pasteur, and S. Cedex, “Hydrothermal Synthesis of Monodisperse Magnetite Nanoparticles”, *Chemistry of Materials*, Vol. 18, pp. 4399–4404, 2006.

18. Morel, A., S. I. Nikitenko, K. Gionnet, A. Wattiaux, J. Lai-kee-him, C. Labrugere, B. Chevalier, G. Deleris, C. Petibois, A. Brisson, M. Simonoff, I. Bordeaux, L. H. Vigneau, and A. Faculte, “Sonochemical Approach to the Synthesis”, *ACS Nano*, Vol. 2, pp. 847–856, 2008.

19. Qu, H., D. Caruntu, H. Liu, and C. J. O’Connor, “Water-Dispersible Iron Oxide Magnetic Nanoparticles with Versatile Surface Functionalities”, *Langmuir*, Vol. 27, pp. 2271–2278, 2011.

20. Fang, M., V. Ström, R. T. Olsson, L. Belova, and K. V. Rao, “Particle Size and Magnetic Properties Dependence on Growth Temperature for Rapid Mixed Co-Precipitated Magnetite Nanoparticles”, *Nanotechnology*, Vol. 23, pp. 145601-145610, 2012.

21. Miles, W. C., J. D. Goff, P. P. Huffstetler, O. T. Mefford, J. S. Riffle, and R. M. Davis, “The Design of Well-Defined PDMS–Magnetite Complexes”, *Polymer*, Vol. 51, pp. 482–491, 2010.

22. Hyeon, T., S. S. Lee, J. Park, Y. Chung, and H. B. Na, “Synthesis of Highly Crystalline and Monodisperse Maghemite Nanocrystallites without a Size-Selection Process”, *Journal of the American Chemical Society*, Vol. 123, pp. 12798–12801, 2001.

23. Tian, Y., B. Yu, X. Li, and K. Li, “Facile Solvothermal Synthesis of Monodisperse Fe_3O_4 Nanocrystals with Precise Size Control of One Nanometre as Potential MRI Contrast Agents”, *Journal of Materials Chemistry*, Vol. 21, p. 2476, 2011.

24. Park, J., K. An, Y. Hwang, J. G. Park, H. J. Noh, J. Y. Kim, J. H. Park, N. M. Hwang, and T. Hyeon, "Ultra-Large-Scale Syntheses of Monodisperse Nanocrystals", *Nature Materials*, Vol. 3, pp. 891–895, 2004.

25. Chen, Z., "Size and Shape Controllable Synthesis of Monodisperse Iron Oxide Nanoparticles by Thermal Decomposition of Iron Oleate Complex", *Synthesis and Reactivity in Inorganic, Metal-Organic, and Nano-Metal Chemistry*, Vol. 42, pp. 1040–1046, 2012.

26. Gupta, A. K. and M. Gupta, "Synthesis and Surface Engineering of Iron Oxide Nanoparticles for Biomedical Applications", *Biomaterials*, Vol. 26, pp. 3995–4021, 2005.

27. Shultz, M. D., J. U. Reveles, S. N. Khanna, and E. E. Carpenter, "Reactive Nature of Dopamine as a Surface Functionalization Agent in Iron Oxide Nanoparticles", *Journal of the American Chemical Society*, Vol. 129, pp. 2482–2487, 2007.

28. Lu, C., L. R. Bhatt, H. Y. Jun, S. H. Park, and K. Y. Chai, "Carboxyl–polyethylene Glycol–phosphoric Acid: A Ligand for Highly Stabilized Iron Oxide Nanoparticles", *Journal of Materials Chemistry*, Vol. 22, p. 19806, 2012.

29. Yuan, W., J. Yuan, L. Zhou, and X. Hong, "Fe_3O_4@poly(2-hydroxyethyl methacrylate)-graft-poly(ε-caprolactone) Magnetic Nanoparticles with Branched Brush Polymeric Shell", *Polymer*, Vol. 51, pp. 2540-2547, 2010.

30. Sun, Y., X. Ding, Z. Zheng, X. Cheng, X. Hu, and Y. Peng, "Surface Initiated ATRP in the Synthesis of Iron Oxide/polystyrene Core/shell Nanoparticles", *European Polymer Journal*, Vol. 43, pp. 762–772, 2007.

31. Ahn, J., D. Moon, and J. Lee, "Arsonic Acid As a Robust Anchor Group for the Surface Modification of Fe_3O_4", *Langmuir*, Vol. 29, pp. 14912-14918, 2013.

32. Yathindranath, V., Z. Sun, M. Worden, L. J. Donald, J. a Thliveris, D. W. Miller, and T. Hegmann, "One-Pot Synthesis of Iron Oxide Nanoparticles with Functional Silane Shells: A Versatile General Precursor for Conjugations and Biomedical Applications", *Langmuir*, Vol. 29, pp. 10850–10858, 2013.

33. Xi, D., X. Luo, Q. Lu, K. Yao, Z. Liu, and Q. Ning, “The Detection of HBV DNA with Gold-Coated Iron Oxide Nanoparticle Gene Probes”, *Journal of Nanoparticle Research*, Vol. 10, pp. 393–400, 2007.

34. Mahmed, N., O. Heczko, A. Lancok, and S. Hannula, “Journal of Magnetism and Magnetic Materials the Magnetic and Oxidation Behavior of Bare and Silica-Coated Iron Oxide Nanoparticles Synthesized by Reverse Co-Precipitation of Ferrous Ion (Fe^{2+}) in Ambient Atmosphere”, *Journal of Magnetism and Magnetic Materials*, Vol. 353, pp. 15–22, 2014.

35. He, W., L. Cheng, L. Zhang, Z. Liu, Z. Cheng, and X. Zhu, “Facile Fabrication of Biocompatible and Tunable Multifunctional Nanomaterials via Iron-Mediated Atom Transfer Radical Polymerization with Activators Generated by Electron Transfer”, *ACS Applied Materials and Interfaces*, Vol. 5, pp. 9663–9669, 2013.

36. Arizaga, A., A. Millán, U. Schubert, and F. Palacio, “Synthesis of Silica-Coated Aqueous Ferrofluids through Ligand Exchange with a New Organosilica Precursor”, *Journal of Material Science*, Vol. 48, pp. 2550–2556, 2012.

37. Earhart, C., N. R. Jana, N. Erathodiyil, and J. Y. Ying, “Synthesis of Carbohydrate-Conjugated Nanoparticles and Quantum Dots”, *Langmuir*, Vol. 24, pp. 6215–6219, 2008.

38. He, X., F. Liu, L. Liu, T. Duan, H. Zhang, and Z. Wang, “Lectin-Conjugated Fe_2O_3@Au Core@Shell Nanoparticles as Dual Mode Contrast Agents for in vivo Detection of Tumor”, *Molecular Pharmaceutics*, Vol. 11, pp. 738-745, 2014.

39. Dai, F., M. Du, Y. Liu, G. Liu, Q. Liu, and X. Zhang, “Folic Acid-Conjugated Glucose and Dextran Coated Iron Oxide Nanoparticles as MRI Contrast Agents for Diagnosis and Treatment Response of Rheumatoid Arthritis”, *Journal of Materials Chemistry B*, Vol. 2, p. 2240, 2014.

40. Jiang, J. S., Z.-F. Gan, Y. Yang, B. Du, M. Qian, and P. Zhang, “A Novel Magnetic Fluid Based on Starch-Coated Magnetite Nanoparticles Functionalized with Homing Peptide”, *Journal of Nanoparticle Research*, Vol. 11, pp. 1321–1330, Oct. 2008.

41. Gaihre, B., M. S. Khil, D. R. Lee, and H. Y. Kim, "Gelatin-Coated Magnetic Iron Oxide Nanoparticles as Carrier System: Drug Loading and in Vitro Drug Release Study", *International Journal of Pharmaceutics*, Vol. 365, pp. 180–189, 2009.

42. Zhu, L., J. Ma, N. Jia, Y. Zhao, and H. Shen, "Chitosan-Coated Magnetic Nanoparticles as Carriers of 5-Fluorouracil: Preparation, Characterization and Cytotoxicity Studies", *Colloids and Surfaces B: Biointerfaces*, Vol. 68, pp. 1–6, 2009.

43. Dong, H., J. Huang, R. R. Koepsel, P. Ye, A. J. Russell, and K. Matyjaszewski, "Recyclable Antibacterial Magnetic Nanoparticles Grafted with Quaternized poly(2-(dimethylamino)ethyl Methacrylate) Brushes", *Biomacromolecules*, Vol. 12, pp. 1305–1311, 2011.

44. Kim, J. S., T. G. Kim, W. H. Kong, T. G. Park, and Y. S. Nam, "Thermally Controlled Wettability of a Nanoporous Membrane Grafted with Catechol-Tethered poly(N-Isopropylacrylamide)", *Chemical Communications (Camb).*, Vol. 48, pp. 9227–9229, 2012.

45. Ohno, K., C. Mori, T. Akashi, S. Yoshida, Y. Tago, Y. Tsujii, and Y. Tabata, "Fabrication of Contrast Agents for Magnetic Resonance Imaging from Polymer-Brush-Afforded Iron Oxide Magnetic Nanoparticles Prepared by Surface-Initiated Living Radical Polymerization", *Biomacromolecules*, Vol. 14, pp. 3453–3462, 2013.

46. Parvin, S., J. Matsui, E. Sato, and T. Miyashita, "Side-Chain Effect on Langmuir and Langmuir-Blodgett Film Properties of poly(N-Alkylmethacrylamide)-Coated Magnetic Nanoparticle", *Journal of Colloid and Interface Science*, Vol. 313, pp. 128–134, 2007.

47. Matsuno, R., K. Yamamoto, H. Otsuka, and A. Takahara, "Polystyrene-Grafted Magnetite Nanoparticles Prepared trough Surface-Initiated Nitroxide-Mediated Radical Polymerization Magnetite", *Chemistry of Materials*, Vol. 15, pp. 3–5, 2003.

48. Chan, N., M. Laprise-Pelletier, P. Chevallier, A. Bianchi, M. A. Fortin, and J. K. Oh, "Multidentate Block-Copolymer-Stabilized Ultrasmall Superparamagnetic Iron Oxide Nanoparticles with Enhanced Colloidal Stability for Magnetic Resonance Imaging", *Biomacromolecules*, Vol. 15, pp. 2146–2156, 2014.

49. Binder, W. H., D. Gloger, H. Weinstabl, E. Pittenauer, M. Chemie, M. U. V, and H. Strasse, “Telechelic Poly(N-Isopropylacrylamides) via Nitroxide-Mediated Controlled Polymerization and ‘Click’ Chemistry: Livingness and ‘Grafting-from’ Methodology”, *Macromolecules*, Vol. 40, pp. 3097–3107, 2007.

50. Yan, K., P. Li, H. Zhu, Y. Zhou, J. Ding, J. Shen, Z. Li, Z. Xu, and P. K. Chu, “Recent Advances in Multifunctional Magnetic Nanoparticles and Applications to Biomedical Diagnosis and Treatment”, *RSC Advances*, Vol. 3, p. 10598, 2013.

51. Basuki, J. S., L. Esser, P. B. Zetterlund, M. R. Whittaker, C. Boyer, and T. P. Davis, “Grafting of P(OEGA) Onto Magnetic Nanoparticles Using Cu(0) Mediated Polymerization: Comparing Grafting ‘from’ and ‘to’ Approaches in the Search for the Optimal Material Design of Nanoparticle MRI Contrast Agents”, *Macromolecules*, Vol. 46, pp. 6038–6047, 2013.

52. Na, H. Bin, G. Palui, J. T. Rosenberg, X. Ji, S. C. Grant, and H. Mattoussi, “Multidentate Catechol-Based Polyethylene Glycol Oligomers Provide Enhanced Stability and Biocompatibility to Iron Oxide Nanoparticles”, *ACS Nano*, Vol. 6, pp. 389–399, 2012.

53. Lu, X., R. Jiang, Q. Fan, L. Zhang, H. Zhang, M. Yang, Y. Ma, L. Wang, and W. Huang, “Fluorescent-Magnetic Poly(poly(ethyleneglycol)monomethacrylate)-Grafted Fe_3O_4 Nanoparticles from Post-Atom-Transfer-Radical-Polymerization Modification: Synthesis, Characterization, Cellular Uptake and Imaging”, *Journal Materials Chemistry*, Vol. 22, p. 6965, 2012.

54. Schmidt, A. M., “The Synthesis of Magnetic Core-Shell Nanoparticles by Surface-Initiated Ring-Opening Polymerization Of Caprolactone”, *Macromolecular Rapid Commununications*, Vol. 26, pp. 93–97, 2005.

55. Qin, S., L. Wang, X. Zhang, and G. Su, “Grafting Poly(ethylene Glycol) Monomethacrylate onto Fe_3O_4 Nanoparticles to Resist Nonspecific Protein Adsorption”, *Applied Surface Science*, Vol. 257, pp. 731–735, 2010.

56. He, X., X. Wu, X. Cai, S. Lin, M. Xie, X. Zhu, and D. Yan, "Functionalization of Magnetic Nanoparticles with Dendritic-Linear-Brush-like Triblock Copolymers and Their Drug Release Properties", *Langmuir*, Vol. 28, pp. 11929–11938, 2012.

57. Chen, F., Z. Cai, Y. Huang, W. Luo, and J. Chen, "Synthesis and Characterization of Copolymer Grafted Magnetic Nanoparticles Radical Polymerization", *Polymer Engineering and Science*, Vol. 53, pp. 956-962, 2013.

58. He, Y., Y. Huang, Y. Jin, X. Liu, G. Liu, and R. Zhao, "Well-Defined Nanostructured Surface-Imprinted Polymers for Highly Selective Magnetic Separation of Fluoroquinolones in Human Urine", *ACS Applied Materials and Interfaces*, Vol. 6, pp. 9634–9642, 2014.

59. Zammarelli, N., M. Luksin, H. Raschke, R. Hergenröder, and R. Weberskirch, "Grafting-from Polymerization of PMMA from Stainless Steel Surfaces by a RAFT-Mediated Polymerization Process", *Langmuir*, Vol. 29, pp. 12834–12843, 2013.

60. Aamer, K. A. and G. N. Tew, "RAFT Polymerization of a Novel Activated Ester Monomer and Conversion to a Terpyridine-Containing Homopolymer", *Journal of Polymer Science, Part A: Polymer Chemistry*, Vol. 45, pp. 5618–5625, 2007.

61. Gurbuz, N., S. Demirci, S. Yavuz, and T. Caykara, "Synthesis of Cationic N-[3-(Dimethylamino)Propyl] Methacrylamide Brushes on Silicon Wafer via Surface-Initiated RAFT Polymerization", *Journal of Polymer Science, Part A: Polymer Chemistry*, Vol. 49, pp. 423–431, 2011.

62. Liu, J., W. Yang, H. M. Zareie, J. J. Gooding, and T. P. Davis, "pH-Detachable Polymer Brushes Formed Using Titanium-Diol Coordination Chemistry and Living Radical Polymerization (RAFT)", *Macromolecules*, Vol. 42, pp. 2931–2939, 2009.

63. Moad, G., E. Rizzardo, and S. H. Thang, "Radical Addition–fragmentation Chemistry in Polymer Synthesis", *Polymer*, Vol. 49, pp. 1079–1131, 2008.

64. Braunecker, W. A. and K. Matyjaszewski, "Controlled/living Radical Polymerization: Features, Developments, and Perspectives", *Progress in Polymer Science*, Vol. 32, pp. 93–146, 2007.

65. Keddie, D. J., “A Guide to the Synthesis of Block Copolymers Using Reversible-Addition Fragmentation Chain Transfer (RAFT) Polymerization.”, *Chemical Society Reviews*, Vol. 43, pp. 496–505, 2014.

66. Moad, G., E. Rizzardo, and S. H. Thang, “Toward Living Radical Polymerization”, *Accounts of Chemical Research*, Vol. 41, pp. 1133–1142, 2008.

67. Willcock, H. and R. K. O’Reilly, “End Group Removal and Modification of RAFT Polymers”, *Polymer Chemistry*, Vol. 1, p. 149, 2010.

68. Li, H., B. Yu, H. Matsushima, C. E. Hoyle, and A. B. Lowe, “The Thiol−Isocyanate Click Reaction: Facile and Quantitative Access to Ω-End-Functional Poly(N,NDiethylacrylamide) Synthesized by RAFT Radical Polymerization”, *Macromolecules*, Vol. 42, pp. 6537–6542, 2009.

69. Scales, C. W., A. J. Convertine, and C. L. McCormick, “Fluorescent Labeling of RAFT-Generated poly(N-Isopropylacrylamide) via a Facile Maleimide-Thiol Coupling Reaction”, *Biomacromolecules*, Vol. 7, pp. 1389–1392, 2006.

70. Thurecht, K. J., I. Blakey, H. Peng, O. Squires, S. Hsu, C. Alexander, and A. K. Whittaker, “Functional Hyperbranched Polymers: Toward Targeted in Vivo ^{19}F Magnetic Resonance Imaging Using Designed Macromolecules”, *Journal of the American Chemical Society*, Vol. 132, pp. 5336–5337, 2010.

71. Moad, G., E. Rizzardo, and S. H. Thang, “End-Functional Polymers, Thiocarbonylthio Group Removal/transformation and Reversible Addition-Fragmentation-Chain Transfer (RAFT) Polymerization”, *Polymer International*, Vol. 60, pp. 9–25, 2011.

72. Moad, G., E. Rizzardo, and S. H. Thang, “Living Radical Polymerization by the RAFT Process A Third Update”, *Australian Journal of Chemistry*, Vol. 65, p. 985, 2012.

73. Heredia, K. L., G. N. Grover, L. Tao, and H. D. Maynard, “Synthesis of Heterotelechelic Polymers for Conjugation of Two Different Proteins”, *Macromolecules*, Vol. 42, pp. 2360–2367, 2009.

74. Roth, P. J., C. Boyer, A. B. Lowe, and T. P. Davis, “RAFT Polymerization and Thiol Chemistry: A Complementary Pairing for Implementing Modern Macromolecular Design”, *Macromolecular Rapid Communications*, Vol. 32, pp. 1123–43, 2011.

75. Nishi, H. and S. Kobatake, “Reduction Reaction to Thiol Group of Dithiobenzoate End Group in Polystyrene Polymerized by Reversible Addition–Fragmentation Chain Transfer”, *Chemistry Letters*, Vol. 37, pp. 630–631, 2008.

76. Roth, P. J., D. Kessler, R. Zentel, and P. Theato, “A Method for Obtaining Defined End Groups of Polymethacrylates Prepared by the RAFT Process during Aminolysis”, *Macromolecules*, Vol. 41, pp. 8316–8319, 2008.

77. Lowe, A. B, B. S. Sumerlin, M. S. Donovan, and C. L. Mccormick, “Facile Preparation of Transition Metal Nanoparticles Stabilized by Well-Defined (Co) Polymers Synthesized via Aqueous Reversible”, *Journal of the American Chemical Society*, Vol. 124 pp. 11562–11563, 2002.

78. Kolb, H. C., M. G. Finn, and K. B. Sharpless, “Click Chemistry: Diverse Chemical Function from a Few Good Reactions”, *Angewandte Chemie International Edition*, Vol. 40, pp. 2004–2021, 2001.

79. Northrop, B. H. and R. N. Coffey, “Thiol-Ene Click Chemistry: Computational and Kinetic Analysis of the Influence of Alkene Functionality”, *Journal of the American Chemical Society*, Vol. 134, pp. 13804–13817, 2012.

80. Tornøe, C. W., C. Christensen, and M. Meldal, “Peptidotriazoles on Solid Phase: [1,2,3]-Triazoles by Regiospecific Copper(i)-Catalyzed 1,3-Dipolar Cycloadditions of Terminal Alkynes to Azides”, *Journal of Organic Chemistry*, Vol. 67, pp. 3057–3064, 2002.

81. Doran, S., E. Murtezi, F. B. Barlas, S. Timur, and Y. Yagci, “One-Pot Photo-Induced Sequential CuAAC and Thiol–Ene Click Strategy for Bioactive Macromolecular Synthesis”, *Macromolecules*, Vol. 47, pp. 3608–3613, 2014.

82. Billiet, L., O. Gok, A. P. Dove, A. Sanyal, L.-T. T. Nguyen, and F. E. Du Prez, "Metal-Free Functionalization of Linear Polyurethanes by Thiol-Maleimide Coupling Reactions", *Macromolecules*, Vol. 44, pp. 7874–7878, 2011.

83. Stolz, R. M. and B. H. Northrop, "Experimental and Theoretical Studies of Selective Thiol-Ene and Thiol-Yne Click Reactions Involving N-Substituted Maleimides", *Journal of Organic Chemistry*, Vol. 78, pp. 8105–8116, 2013.

84. Zhu, J., J. Chin, C. Wängler, B. Wängler, R. B. Lennox, and R. Schirrmacher, "Rapid (18)F-Labeling and Loading of PEGylated Gold Nanoparticles for in Vivo Applications", *Bioconjugate Chemistry*, Vol. 25, pp. 1143–1150, 2014.

85. Neubert, B. J. and B. B. Snider, "Synthesis of (+/-)-Phloeodictine A1", *Organic Letters*, Vol. 5, pp. 765–768, 2003.

86. Shepherd, J. L., A. Kell, E. Chung, C. W. Sinclar, M. S. Workentin, and D. Bizzotto, "Selective Reductive Desorption of a SAM-Coated Gold Electrode Revealed Using Fluorescence Microscopy", *Journal of the American Chemical Society*, Vol. 126, pp. 8329–8335, 2004.

87. Verdoes, M., U. Hillaert, B. I. Florea, M. Sae-Heng, M. D. P. Risseeuw, D. V Filippov, G. a van der Marel, and H. S. Overkleeft, "Acetylene Functionalized BODIPY Dyes and Their Application in the Synthesis of Activity Based Proteasome Probes", *Bioorganic and Medicinal Chemistry Letters*, Vol. 17, pp. 6169–6171, 2007.

88. Santi, D. V, E. L. Schneider, R. Reid, L. Robinson, and G. W. Ashley, "Predictable and Tunable Half-Life Extension of Therapeutic Agents by Controlled Chemical Release from Macromolecular Conjugates", *Proceedings of National Academy of Sciences U.S.A.*, Vol. 109, pp. 6211–6216, 2012.

89. Lai, J. T., D. Filla, and R. Shea, "Functional Polymers from Novel Carboxyl-Terminated Trithiocarbonates as Highly Efficient RAFT Agents", *Macromolecules*, Vol. 35, pp. 6754–6756, 2002.

90. Zhen, G., B. W. Muir, B. a. Moffat, P. Harbour, K. S. Murray, B. Moubaraki, K. Suzuki, I. Madsen, N. Agron-Olshina, L. Waddington, P. Mulvaney, and P. G.

Hartley, “Comparative Study of the Magnetic Behavior of Spherical and Cubic Superparamagnetic Iron Oxide Nanoparticles”, *Journal of Physical Chemistry C*, Vol. 115, pp. 327–334, 2011.

91. Lv, W., L. Liu, Y. Luo, X. Wang, and Y. Liu, “Biotinylated Thermoresponsive Core Cross-Linked Nanoparticles via RAFT Polymerization and ‘Click’ Chemistry”, *Journal of Colloid and Interface Science*, Vol. 356, pp. 16–23, 2011.

92. Xiao, Z. P., K. M. Yang, H. Liang, and J. Lu, “Synthesis of Magnetic, Reactive, and Thermoresponsive Fe3O4 Nanoparticles via Surface-Initiated RAFT Copolymerization of N-Isopropylacrylamide and Acrolein”, *Journal of Polymer Science Part A: Polymer Chemistry*, Vol. 48, pp. 542–550, 2010.

93. Zobrist, C., J. Sobocinski, J. Lyskawa, D. Fournier, V. Miri, M. Traisnel, M. Jimenez, and P. Woisel, “Functionalization of Titanium Surfaces with Polymer Brushes Prepared from a Biomimetic RAFT Agent”, *Macromolecules*, Vol. 44, pp. 5883–5892, 2011.

94. Xu, C., K. Xu, H. Gu, R. Zheng, H. Liu, X. Zhang, Z. Guo, and B. Xu, “Dopamine as a Robust Anchor to Immobilize Functional Molecules on the Iron Oxide Shell of Magnetic Nanoparticles”, *Journal of the American Chemical Society*, Vol. 126, pp. 9938–9939, 2004.

95. Rajh, T., L. Chen, and K. Lukas, “Surface Restructuring of Nanoparticles: An Efficient Route for Ligand-Metal Oxide Crosstalk”, *Journal of Physical Chemistry B*, Vol. 106, pp. 10543–10552, 2002.

96. Moad, G., Y. K. Chong, A. Postma, E. Rizzardo, and S. H. Thang, “Advances in RAFT Polymerization: The Synthesis of Polymers with Defined End-Groups”, *Polymer*, Vol. 46, pp. 8458–8468, 2005.

97. Fan, Q.-L., K.-G. Neoh, E.-T. Kang, B. Shuter, and S.-C. Wang, “Solvent-Free Atom Transfer Radical Polymerization for the Preparation of Poly(poly(ethyleneglycol) Monomethacrylate)-Grafted Fe_3O_4 Nanoparticles: Synthesis, Characterization and Cellular Uptake”, *Biomaterials*, Vol. 28, pp. 5426–5436, 2007.

98. Bontempo, D., K. L. Heredia, B. Fish, and H. D. Maynard, “Cysteine-Reactive Polymers Synthesized by Atom Transfer Radical Polymerization for Conjugation to Proteins”, *Journal of the American Chemical Society*, Vol. 126, pp. 15372–15373, 2004.